NTNU
Norwegian University of
Science and Technology

Isogeometric analysis with trimmed geometries applied to ship hulls

Sofie Schønfeldt-Borchgrevink

Marine Technology
Submission date: June 2018
Supervisor: Josef Kiendl, IMT

Norwegian University of Science and Technology
Department of Marine Technology

NTNU

Norwegian University of Science and Technology

Master Thesis

Isogeometric Analysis with Trimmed Geometries Applied to Ship Hulls

by Sofie Schønfeldt-Borchgrevink

Department of Marine Technology

Faculty of Engineering Science and Technology

Norwegian University of Science and Technology

2018

Abstract

This Paper aims to investigate Trimmed NURBS surfaces for Isogeometric Analysis(IGA). NURBS are Non-Rational B-spline functions which are widely used for geometric modelling in most Computer aided Design programs. This is because they have the ability to represent a wide range of curves, surfaces and solids. When models are created in CAD and imported in to Finite Element programs for analysis, the geometry is approximated, and the resulting model is less accurate. IGA aims to close the gap between design and analysis by performing analysis directly on the geometry from CAD. IGA therefore also use NURBS in analysis. A walk-through of the theory behind NURBS curves and surfaces are presented in this paper.
One problem with IGA is that trimming is a very common practice when constructing complex geometries in CAD. Trimming does not actually change the mathematical description of the surface, it simply renders the trimmed part invisible. This means that when analysis is performed on a trimmed surface, the surface will behave exactly like the surface before the trimming. The main purpose of this thesis is to investigate how to perform analysis on trimmed NURBS surfaces. A trimmed surface consist of a trimming curve and an untrimmed surface. The parametric coordinates of the two are different, and so a correlation between the two must be found.
Trimmed elements are classified into different cases based on the location of the trimming curves relative to the element vertex points. Searching steps to find out which elements are trimmed, untrimmed or inactive is explained, and the intersection points between the elements and the trimming curves can be found. Classifying the elements and determining the intersection points are important for the analysis.
Analysis of trimmed NURBS surfaces is possible through the use of mapping. Different mapping schemes are discussed and used. The blending function method divides the trimming curves into segments based on their intersection with the elements, and maps element that are quadrilateral or triangular in shape. The Adaptive Gaussian integration procedure shifts, scales and rotates the trimming curves into a Gaussian space, and constructs an element. Integration points are found on the Adaptive Gaussian surface. Nurbs enhances triangles uses several mapping to map a triangular domain with a NURBS curve from the Gaussian space.
Finally, analysis of ship hulls are discussed. Ship hulls are composed of many small components. Global analysis is usually performed on the whole structure, while local analysis is important to investigate the behaviour of the hull accurately. A trimmed element representing a plate with a hole is investigated by Isogeometric analysis of trimmed and untrimmed surfaces as well as Finite elemen analysis. Isogeometric analysis holds an advantage to FEA in both accuracy and computational time. The results converge for a much coarser mesh. The one advantage FE has over IGA is that if the element can not be trimmed, creating the model in CAD might be much more time consuming. The trimmed IGA also proves stable, and so with further investigation and development of the trimmed analysis IGA might prove far superior to FEA,

Contents

Chapter 1

Introduction

Analysis of ship hulls are crucial for designing a ship that is stable, can carry the desired load, has an efficient geometry with low resistance and many other aspects. The curved geometry of the hull created a lot of challenges for analyzing the geometry accurately in standard FEA programs. Because shells are curved arbitrarily in 3D, and the appropriate description necessary, it is vulnerable to large errors for a FE analysis. Meshing of the structure changes the geometry, and in addition mesh refinement are time consuming. Isogeometric analysis is an alternative analysis method to FEA, where the original geometry is preserved, and the need for meshing is eliminated. This method therefore aim to improve the accuracy of an analysis, as well as serve as a tool to save time.

Isogeometric analysis is more related to CAD, than FEM, which makes the implementation between a CAD program and the analysis easier. Both are based on polynomial curves, and so the geometry created on which the analysis is performed is exactly the same as the original geometry. Isogeometric analysis (IGA) uses spline functions from Computer Aided Design(CAD) in the analysis of a model. Most commonly used in CAD are NURBS. NURBS curves and surfaces are a combination of control points, with corresponding weights, and basis function over a parametric space. The basis functions are derived from knots vectors, which define a parametric space, and a polynomial degree. The goal of IGA is to merge CAD and FEA into and thus to close the gap between design and analysis. IGA holds advantages to FEA especially for models where the geometric representation requires high accuracy, such as for shells, because the analysis is performed on the exact geometry from CAD. In addition, the process of meshing is avoided. A common tool in the design process is trimming, where a part of the surface or curve is cut away. This is especially useful when designing complex models because you do not have to change the surface or curve description in any way. The fact that the geometric description is not changed is also why trimming is one of the problems IGA has encountered. The control points, knot vectors and basis functions remain the same, while the trimmed part has only been made invisible. Avoiding trimming altogether in the design process is one solution, but for complex models this would be time consuming and thus eliminating one of the major advantages to IGA. Several methods to incorporate the trimming curve in the analysis has been proposed, thus making IGA possible for designs where trimming has been used.

The purpose of this thesis is to consider relevant geometries for ship hulls and perform trimmed IGA on these type of models. A set of matlab codes have been written, which implements several methods proposed for analysis of trimmed elements. The code imports the surface and trimming curves from an IGES file, categorizes the element into the possible cases, find the intersection points and does refinement for elements not suited for analysis. Analysis can be performed using three different mapping methods. Various conditions for each method is implemented by the code. This code is the basis for this thesis, and all plots and results are obtained by this.

Chapter 2

Geometric Modeling and Fundamentals

Geometric shapes are described mathematically, thus it is important to have functions which can describe a wide range of geometric shapes. A parametric description offers the most suitable representation of geometries, and are thus the basis for geometric modelling today. For a parametric curve, the coordinates (x,y,z) are explicit functions of an independent parameter.
Computer Aided Design(CAD) is mostly used for designing geometric models. Standard for CAD programs is that they use NURBS functions for modelling. NURBS are Non-Uniform Rational B-Splines, which describe a curve, surface or solid as linear combinations of Basis functions and control points over a parametric space.

2.1 NURBS

NURBS are based on B-splines which in turn are based on Bézier curves.

2.1.1 Bézier curves

Bézier curves are described as

$$\mathbf{C}(u) = \sum_{i=1}^{n} B_{i,l}(u)\mathbf{P}_i, \tag{2.1}$$

where $\mathbf{P}_i$ are the control points, l is the polynomial degree,n is the number of control points and $B_{i,l}$ are the basis functions:

$$B_{i,l} = \frac{n!}{i!(n-i)!} u_i (1-u)^{n-i}. \tag{2.2}$$

The polynomial degree and the number of control points are related through l=n-1. This means that when the number of control points increase, the polynomial degree increases linearly. Another disadvantage to this representation is that all control points are related to each other and alteration of one point would affect the whole curve. B-splines were introduced as a solution to this.

2.1.2 B-Splines

For B-Splines. the parameter space is divided into knot spans, making the degree independent to the number of control points. An important property of B-spline curves is that the control point at the start and end of the curve only has influence on their respective knot spans. All other control points influences a maximum of l+1 knot spans.

Knot vectors

A knot vector, $U = [u_1, u_2, ..., u_{n+l+1}]$, defines the parametric space, where u_i are parametric coordinates in ascending order. Each distinguishable coordinate divides the curve into knot spans.

Inside a knot span, there is always C^∞ continuity. At a knot, there is C^{l-k} continuity, where k is the number of repeated knots. At the beginning and end of a curve, there should be C^{-1} continuity, meaning that the knots usually have a multiplicity of l+1 here. These are called open knot vectors. Curves with open knot vectors are always interpolated at the first and last control points, which is advantageous when modeling because the beginning and end of the curve can be easily determined.
Figure 2.1 shows a B-Spline curve, $\mathbf{C}(u)$, with three inner knots: u_5, u_6 and u_7. The knots divide the curve into four knot spans. The knots are marked with an x. The dashed line shows the control point polygon, which connects the control points, P_i.

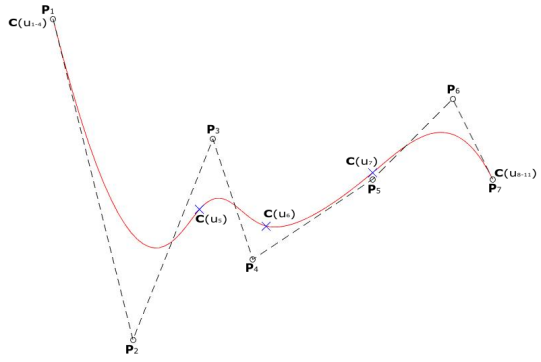

Figure 2.1: Curve with knot vector U=[0 0 0 0 0.25 0.5 0.75 1 1 1 1], and polynomial degree l=3.

If the multiplicity at an inner knot is equal to the polynomial degree, there is C^0 continuity, meaning that the curve is interpolated at this knot. Figure 2.2 shows a B-Spline curve with control points, P_i, control polygon and knot spans. The multiplicity at the inner knot, u_{5-7} is equal to the polynomial degree, and the curve is interpolated at this knot.

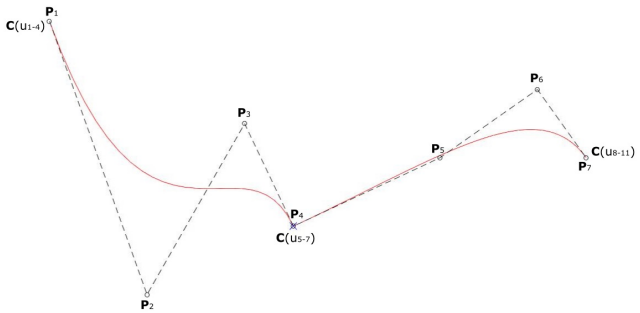

Figure 2.2: Curve with knot vector U=[0 0 0 0 0.5 0.5 0.5 1 1 1 1], and polynomial degree l=3.

For B-spline surfaces, there are two knot vectors, $S = [s_1, s_2, ..., s_{n+1+p}]$ and $T = [t_1, t_2, ..., t_{m+1+p}]$.
The surfaces consists of a control point net with n x m control points, the two knot vectors and two polynomial degrees p and q.
Figure 2.3 shows a surface and its corresponding knots, control points and control point net. The inner knots in s- and t-direction divide the surface into four patches.

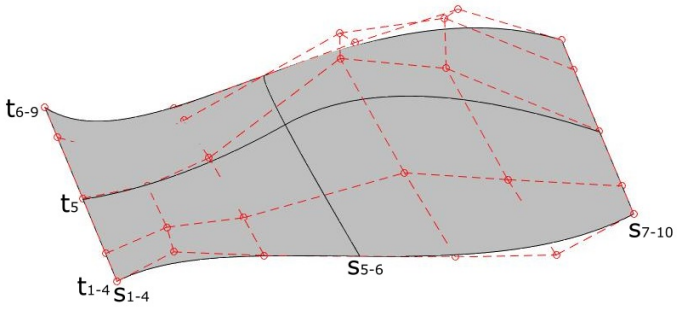

Figure 2.3: Surface with knot vectors S=[0 0 0 0 0.5 0.5 1 1 1 1], T=[0 0 0 0 0.5 1 1 1 1] and polynomial degrees p=q=3.

Basis functions

The knot vectors and polynomial degrees are used to determine the basis functions, N_i. First, the B-Spline basis function is computed for l=0.

$$N_{i,0}(u) = \begin{cases} 1, & u_i \leq u < u_{i+1} \\ 0, & otherwise \end{cases} \tag{2.3}$$

For l $\geq$ 1, The basis functions are

$$N_{i,l}(u) = \frac{u - u_i}{u_{i+l} - u_i} N_{i,l-1}(u) + \frac{u_{i+l+1} - u}{u_{i+l+1} - u_{i+1}} N_{i+1,l-1}(u) \tag{2.4}$$

The first derivative of the basis function is

$$N'_{i,l}(u) = \frac{l}{u_{i+l} - u_i} N_{i,l-1}(u) - \frac{l}{u_{i+l+1} - u_{i+1}} N_{i+1,l-1}(u) \tag{2.5}$$

Figure 2.4 shows the basis functions for the curve in Figure 2.1.

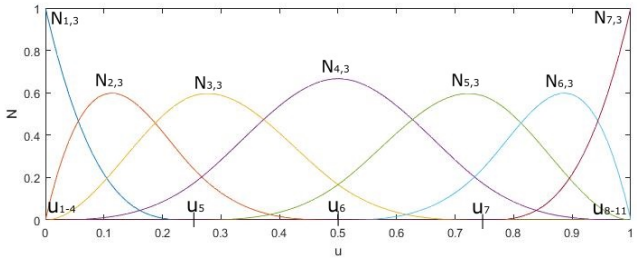

Figure 2.4: Basis functions for the curve in figure 2.1

As mentioned previously, the basis functions are C^{∞} continuous inside knot spans and C^{l-k} continuous at knots of multiplicity k. If a basis function has C^0 continuity at a knot, the basis function will be one, while the rest will be zero at this knot.
The curve in Figure 2.2 has multiplicity k=3 at u=0.5 and degree l=3, which can be seen in Figure 2.5. The basis function $N_{4,3}$ is 1, while the rest are 0 at u_{5-7}

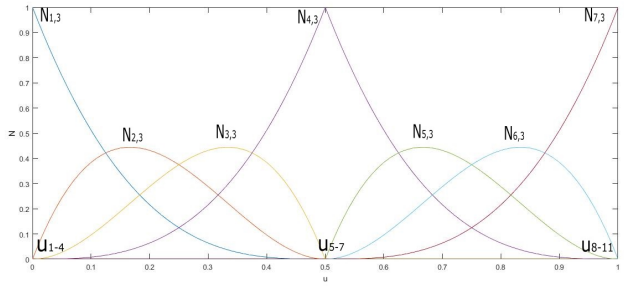

Figure 2.5: Basis functions for the curve in figure 2.2

B-Spline basis functions have the following important properties:

1. $N_{i,l}(u) \neq 0$ only in interval $[u_i, u_{i+l+1}]$.
2. $\sum_{i=1}^{n} N_{i,l}(u) = 1$
3. $N_{i,l}(u) \geq 0$
4. $\sum_{i=1}^{n} \alpha_i N_{i,l}(u) = 0 \Leftrightarrow \alpha_i = 0$, i=1,2,...,n

B-spline Curves and surfaces

B-spline curve are described by a set of control points, $\mathbf{P}_i$ and basis functions $N_{i,l}(u)$ as:

$$\mathbf{C}(u) = \sum_{i=1}^{n} N_{i,l}(u)\mathbf{P}_i \tag{2.6}$$

The first derivative of B-spline curves are

$$\mathbf{C}'(u) = \sum_{i=1}^{n} N'_{i,l}(u)\mathbf{P}_i \tag{2.7}$$

B-Spline surfaces are defined by two basis functions, $N_{i,p}(s)$ and $M_{j,q}(t)$, and a net of control points with n control points in s-direction and m control points in t-direction.

$$\mathbf{S}(s,t) \sum_{i=1}^{n} \sum_{j=1}^{m} N_{i,p}(s) M_{j,q}(t) \mathbf{P}_{i,j} \tag{2.8}$$

2.1.3 NURBS

NURBS stand for Non-Uniform Rational B-splines. They differ from B-splines in that their knot vector in general is not uniform, and that their basis functions are piece-wise rational polynomials.
Each control point of a NURBS curve or surface has a corresponding weight, w_i. This weight enables the further opportunities in geometric modelling, in particular the creation of circles and ellipses.
A NURBS curve is represented as:

$$\mathbf{C}(u) = \frac{\sum_{i=1}^{n} N_{i,l}(u) w_i \mathbf{P}_i}{\sum_{i=1}^{n} N_{i,l}(u) w_i} \tag{2.9}$$

The NURBS basis functions can be expressed as

$$R_{i,l}(u) = \frac{N_{i,l}(u) w_i}{\sum_{i=1}^{n} N_{i,l}(u) w_i}, \tag{2.10}$$

so the curve can be represented as a function of the basis function and the control points:

$$\mathbf{C}(u) = \sum_{i=1}^{n} R_{i,l}(u) \mathbf{P}_i \tag{2.11}$$

For NURBS surfaces, the basis function is defined as

$$R_{ij}^{pq}(s,t) = \frac{N_{i,p}(s) M_{j,q}(t) w_{i,j}}{\sum_{i=1}^{n} \sum_{j=1}^{m} N_{i,p}(s) Mj,q(t) w_{i,j}} \tag{2.12}$$

NURBS curves and surfaces where all weights, w_i are equal are B-spline curves and surfaces.
Figure 2.6 (a) shows a NURBS curve representing a circle with weights w_k=0.707 at control points $\mathbf{P}_k$, k=2,4,6,8.

Figure 2.6 (b) shows the curve with the same knot vector, degree and control points, but with uniform weights $w_i = 1$, i=1,2,..,9.

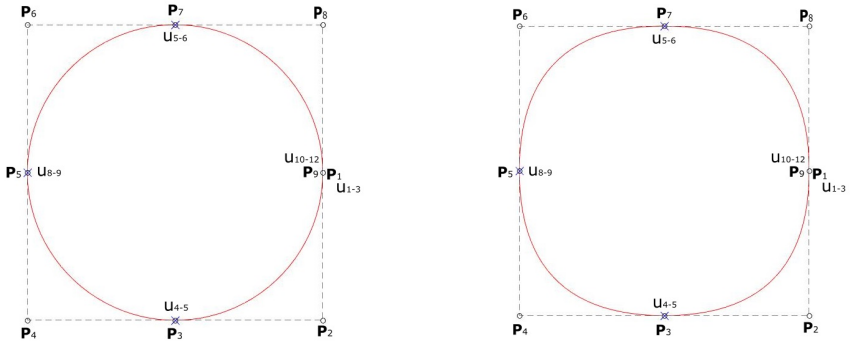

(a) NURBS curve with non-uniform weight (b) B-Spline curve

Figure 2.6: Circle with knot vector U=[0 0 0 0.25 0.25 0.5 0.5 0.75 0.75 1 1 1] ans degree l=2

Chapter 3

Trimmed surfaces

3.1 Representation of Trimmed Surfaces

The trimming operation in CAD modifies which part of the surface is visible, but the parameters used to describe the surface mathematically remains unchanged.
A trimmed surface is described by the untrimmed surface and a set of trimming curves. The direction of the trimming curves determine which part of the surface is in material region and which part is in void region: Void region is to the right of the direction of increasing knot values. The trimming curves all form closed loops, so that the entire boundary of the trimmed surface can be represented by a set of M trimming curves. In addition, there can be inner trimming curves.
A distinction between inner and outer trimming curves is the direction of the curves: Inner trimming curves has a direction that moves clockwise, while the direction of outer trimming curves are counterclockwise.

The surface and the trimming curves use a different set of parameters, thus making it challenging to relate the two. Surfaces are described by the two parameters (s,t), while curves are described by only one parameter, (u). In parameter space, curves are related to the parameters (s,t) by:

$$\mathbf{C}_k^{Pa}(u) = \begin{bmatrix} s_k(u) \\ t_k(u) \end{bmatrix} = \sum_{i=1}^{n_k} R_{i,l}(u)\mathbf{P}_i^{Pa,k}, \qquad k = 1,2,..,M \tag{3.1}$$

Where $\mathbf{P}_i^{Pa,k}$ are the control points of the trimming curve in parametric space, M is the number of trimming curves, l is the polynomial degree and u curve parameter. s_k and t_k are the parameters of the curve on the surface.
Figure 3.1 shows the parameter space of a trimmed surface with knot vectors U=V=[0 0 0 0 0.25 0.5 0.75 1 1 1 1] and polynomial degree p=q=3. There are six trimming curves which form two closed loops; one inner and one outer. Five of the curves represent the outer boundary, while the last, $\mathbf{C}_6$ describes the inner.
The orientation of the inner boundary is clockwise, while the outer are counter-clockwise. Trimming curves 2,3,4 and 5 lie on the boundary of the untrimmed surface and does not actually contribute to the trimming of the surface.

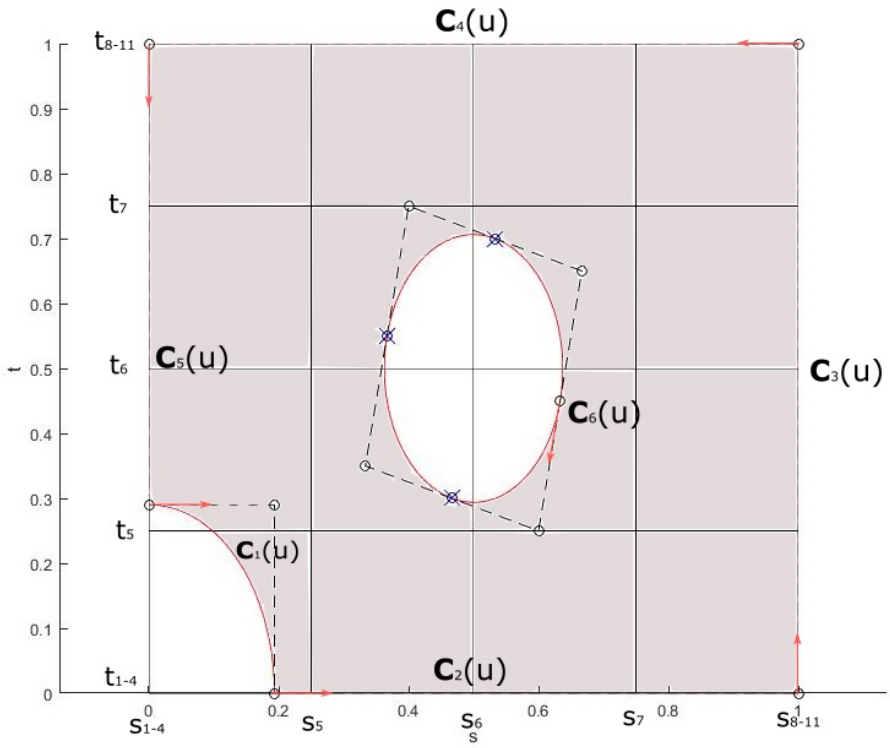

Figure 3.1: Trimmed surface in parameter space described by the trimming curves, $\mathbf{C}_i$

The untrimmed surface in physical space is:

$$\mathbf{S}(s,t) = \sum_{i=1}^{n}\sum_{j=1}^{m} R_{ij,pq}(s,t)\mathbf{P}_{ij}, \tag{3.2}$$

The trimmed surface is defined by the domain, $\mathcal{D}$, which is represented by the trimming curves

$$\begin{aligned} \mathbf{S}_{visible} &= \{\mathbf{S}(s,t)|(s,t) \in \mathcal{D}\}, \\ \mathcal{D} &= \bigcup \mathbf{C}_k \end{aligned} \tag{3.3}$$

The curves which bound the surface in physical space can be found by mapping the parametric coordinates, $(s_k(u), t_k(u))$, found from Eq.3.1 to the untrimmed surface, $\mathbf{S}(s,t)$

$$\begin{aligned} \mathbf{C}_k^{Ph}(u) &= \mathbf{S}(s_k(u), t_k(u)), \\ k &= 1,2,..,M \end{aligned} \tag{3.4}$$

The surface from Figure 3.1 is plotted in physical space, and shown in figure 3.2.

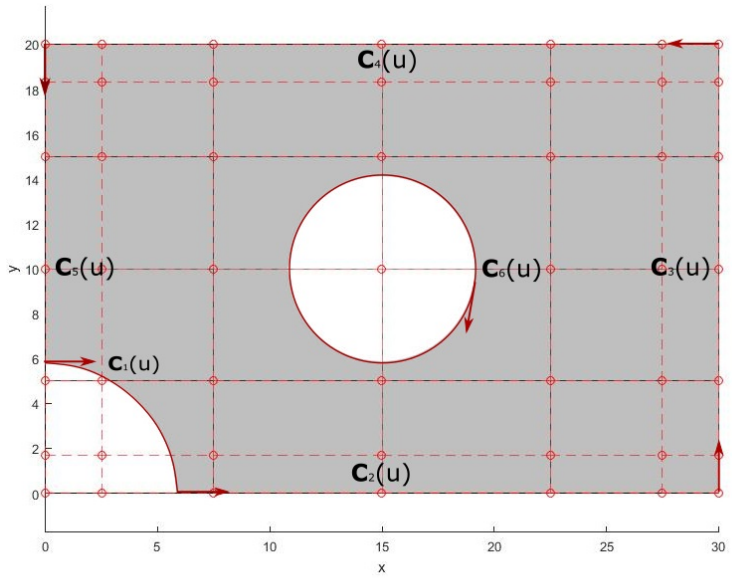

Figure 3.2: Trimmed surface in physical space described by the trimming curves, $\mathbf{C}_i$

The two major challenges to trimmed elements in Isogeometric Analysis are how to relate the trimming curves to the surface in order to determine which part of the surface is trimmed, and how to perform analysis on trimmed elements. The first will be addressed in this section, while the latter will be addressed in chapter 4.

3.2 Classification of Trimmed Elements

Each element of the untrimmed domain need to be classified as either trimmed or untrimmed. Untrimmed elements have no trimming curves within their boundary. Further, untrimmed elements are classified as active or inactive based on whether they lie within the trimmed domain.
Inactive elements are completely outside the trimmed domain, and they will in no way contribute to the stiffness matrix. Untrimmed, active elements are treated in the same way in the integration of the stiffness matrix as for conventional IGA.
For trimmed elements, the next step is to determine which parts of the element is trimmed and thus how the Gauss integration points should be distributed.
Each trimmed element is classified into different cases based on which parts of the element is trimmed. Two searching steps have been proposed for such classification.

3.2.1 The First Searching step

Figure 3.3 shows the first searching step for classifying the elements.

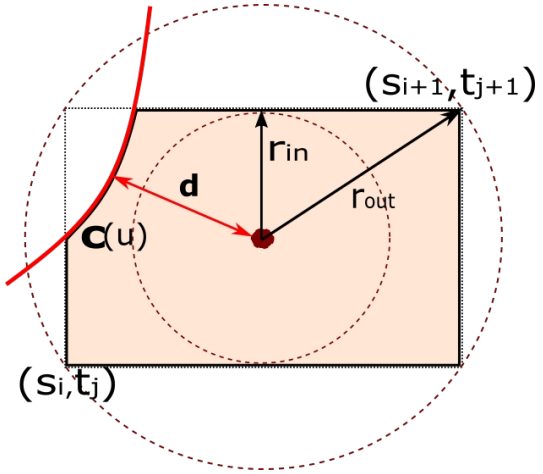

Figure 3.3: First searching step for classifying elements.

The shortest distance from the trimming curve to the middle of the element is found. The inner and outer radius are defined as:

$$r_{in} = min\{\frac{s_{i+1} - s_i}{2}, \frac{t_{j+1} - t_j}{2}\} \tag{3.5}$$

$$r_{out} = \frac{1}{2}\sqrt{(s_{i+1} - s_i)^2 + (t_{j+1} - t_j)^2} \tag{3.6}$$

Based on the relation between the length of the distance vector, $|\mathbf{d}|$, the inner radius, r_{in}, and the outer radius, r_{out}, we can draw the following conclusions:

1. If $r_{in} > |\mathbf{d}|$, the element is trimmed.
2. If $r_{out} < |\mathbf{d}|$, the element is untrimmed.
3. If $r_{in} \leq |\mathbf{d}| \leq r_{out}$, it is unknown whether the element is trimmed or not.

If the first searching step provides information that the element is untrimmed, it is necessary to further classify the element as active or inactive. This is determined by finding the cross product between the distance vector, $\mathbf{d}$ and the tangential vector of the trimming curve,$\mathbf{v}$, at the point closest to the centre of the element. The tangential vector can be found as the derivative of the trimming curve.

$$\mathbf{v} = \mathbf{C}'(u_c), \tag{3.7}$$

where u_c is the parameter of the trimming curve at the closest point to the centre of the element. The element is inactive if $\mathbf{d} \times \mathbf{v}$ is negative, otherwise it is active. Figure 3.4 shows an untrimmed element where the direction of the trimming curve and its placement relative to the element leads to a negative cross product. The element is therefore inactive.

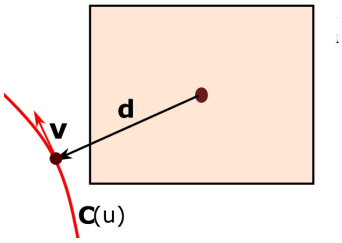

Figure 3.4: Classification of active or inactive element for first searching step.

3.2.2 The Second Searching Step

If the element is trimmed or unknown, a second searching step is required. For this step, each vertex point is used for reference instead of the middle-point.

The shortest distance vector, $\mathbf{d}_i$, for each vertex point if found along with the corresponding tangential vector, $\mathbf{v}_i$. Again the cross-product $\mathbf{d} \times \mathbf{v}$ determines if the vertex point is active or inactive.
If the cross-product is zero, there is an intersection point between the trimming curve and the element at the vertex-point.
Figure 3.5 depicts a trimmed element with a trimming curve which leaves only vertex-point 2 active.

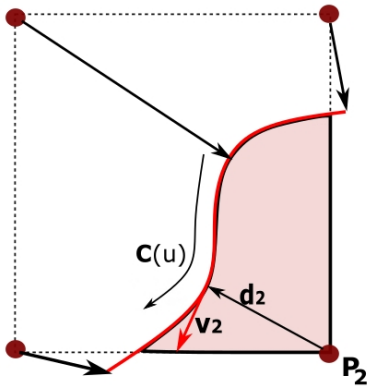

Figure 3.5: Second searching step for classification of elements.

3.2.3 The Trimmed Element Cases

If between 1 and 3 vertex points are active, the element can be classified into three main trimming cases:

1. One vertex-point is active, while the remaining vertex-points can be inactive or lie at an intersection point. There are four sub-cases corresponding to this case; one for each vertex point that can be active. An element represented by this case is shown in figure 3.6 (a), where vertex point 2,3 and 4 are active.

2. Two vertex points are active. The remaining can be inactive or lie at an intersection point. One exception is if two vertex points are active, while the other two are at the intersection points;which means the element is untrimmed.
   For the case of two active vertex-points, it is important that the active vertex points are neighbouring points, as shown in Figure 3.6 (b).
   Cases where this does not apply will be discussed later. There are four sub-cases, one for each possible combination of two active neighbouring vertex-points.

3. Three vertex-points are active, while the fourth must be inactive. If the fourth lies at an intersection point, the element is untrimmed. There are four sub-cases, one for each vertex point which is inactive.
   An example of this element is shown in Figure 3.6 (c), where vertex point 1 is active.

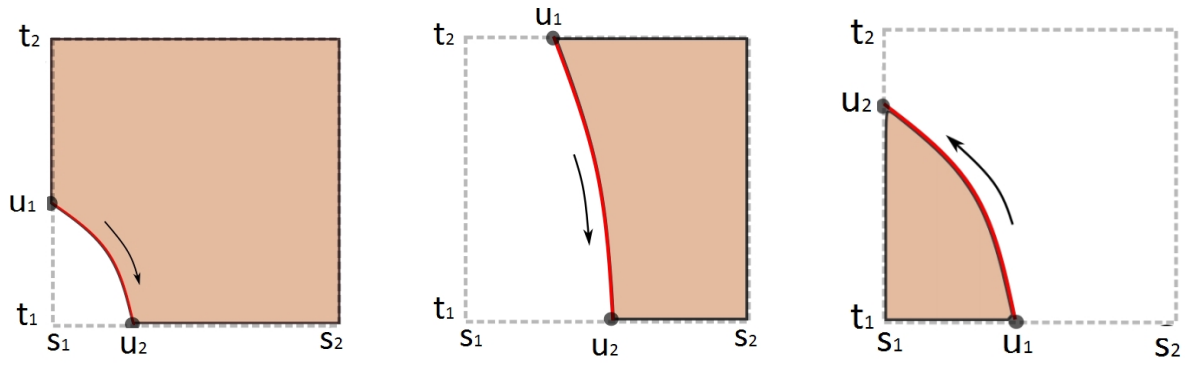

(a) (b) (c)

Figure 3.6: Determining intersection points for the element cases: (a) One inactive vertex point; (b) Two inactive vertex points; (c) Three inactive vertex points

3.3 Intersection Points

In order to determine which part of the trimming curve lies within each element, the intersection points need to be located. These points are where the trimming curve enters and exits the element.
Since the element is defined in terms of (s,t), while the curve has coordinate u in parametric space, iteration to a satisfactory solution is necessary. Figure 3.7 shows two trimmed elements of case 1 and 2 in parametric space.

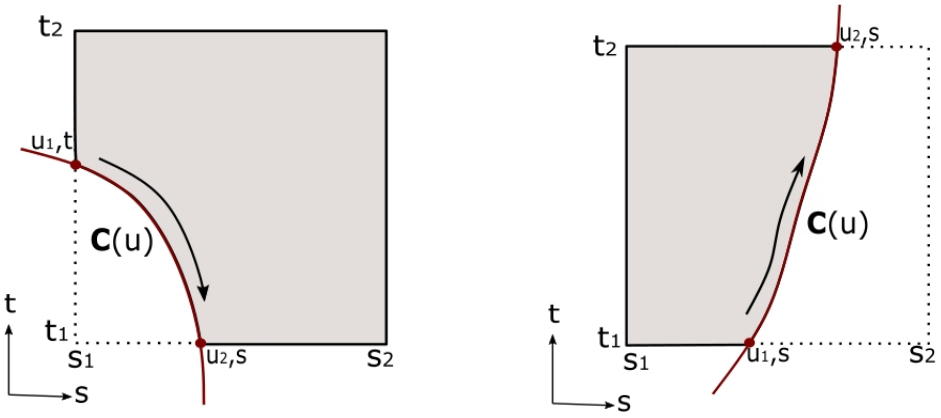

(a) (b)

Figure 3.7: Finding intersection points between trimming curve and element: (a) Type 1 (b) Type 2.

For figure 3.7 (a) at the first intersection point, u_1, we know that $s = s_1$. Then we have the following relation:

$$s_1 = \mathbf{C}(u) \tag{3.8}$$

u_1 is the u-value where Eq.3.8 is true. With the intersection point in terms of the curve found, the unknown coordinate for intersection point on the element is:

$$t = \mathbf{C}_t(u_1) \tag{3.9}$$

When the element case and active vertex points are known, similar methods can be applied to all the element cases mentioned previously.

3.3.1 Special cases

There are some cases of trimmed elements where the boundaries of the trimming curves do not define an element case suitable for analysis. The classification of elements described in this thesis require at least one vertex point to lie within the void region.
Closed curves inside an element is one case where no vertex points are in void region, but the element is still trimmed, as shown in Figure 3.8
The first searching step will classify the element as trimmed, but the second will classify it as untrimmed. In order to properly classify the Element and perform analysis, refinement is necessary.

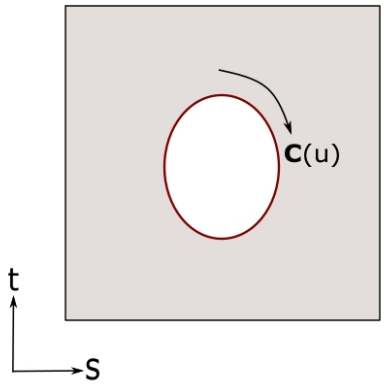

Figure 3.8: Closed trimming curve inside element

Another case is when the trimming curve crosses an edge, but no vertexes, as is the case in the first element in Figure 3.9. It could be possible to classify the element as trimmed based on the first searching step and then search the curve for any points lying on either edge, but for simplicity, refinement is done on these type of elements.

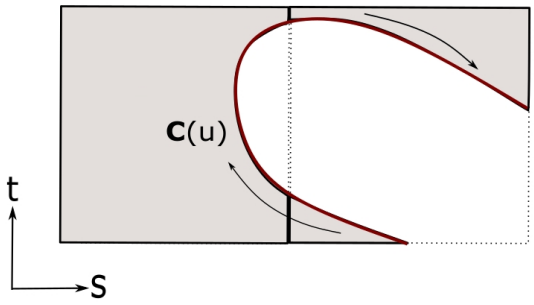

Figure 3.9: Second searching step for classification of elements.

The other element in Figure 3.9 depicts another special case: the trimming curve exits the element and enters back in. This type of element poses a difficult scenario because vertex points 1,3 and 4 are active, meaning the element would be classified as case 1.
There are certain requirements for trimmed elements to be eligible for analysis: The sign of the tangential vector at any point on the trimming curve can not differ from the sign of the tangential vector at the start of the trimming curve in both s- and t-direction. This is called undercuts, and in the case for the element in Figure 3.9, there are undercuts in both directions. To find out if an element has undercuts, a searching step finds the derivatives of the trimming curve at multiple steps along the curve and where they change.
Figure 3.10 shows two trimmed surfaces in parametric space along with the tangential vector at any location where there are undercuts. As soon as an undercut is detected, this point becomes the new starting point for

comparison. The direction of the trimming curve in Figure 3.10 (b) changes three times for the element, but only in t-direction. This surface is therefore eligible for analysis. The surface in Figure 3.10 (a), however, has undercuts in both s- and t-direction, and refinement is necessary. The element can either be divided into equal parts until the condition is satisfied, or refinement can be done along the location of where the undercuts are found.

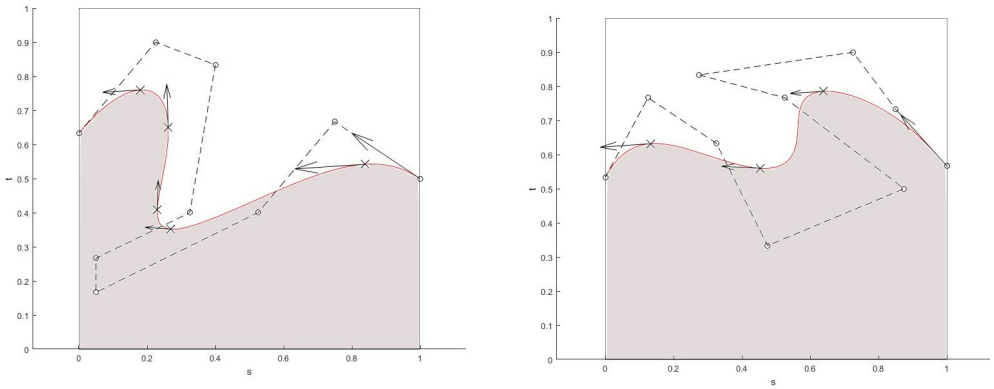

(a) (b)

Figure 3.10: Locating points along the curve where the direction of the tangential vector changes.

Another special case, is when there are two trimming curves inside one element, as shown in Figure 3.11. The searching steps for determining the element cases mentioned previously are performed on each curve separately so it is possible to classify the element with two separate cases and subdivide the single element during analysis. Subdivision could be performed between the two curves vertically or horizontally if

$$\mathbf{C}_s^I(u_2) \leq \mathbf{C}_s^{II}(u_2), \tag{3.10}$$

or

$$\mathbf{C}_t^I(u_1) \leq \mathbf{C}_t^{II}(u_1), \tag{3.11}$$

where u_1 and u_2 are the intersection points of the trimming curves. An example of a subdivision of this element is represented as a stippled, vertical line.

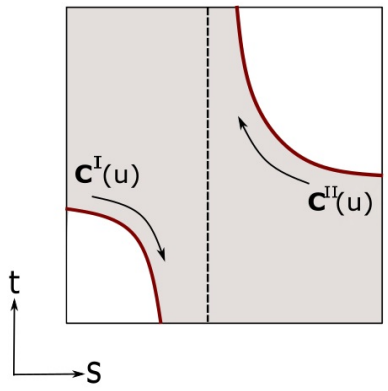

Figure 3.11: Two trimming curves with subdivision in vertical direction.

Chapter 4

Basis for Analysis

4.1 Analysis of Shells

Shell formulations focus mainly on effects which are relevant for shell structures. This is advantageous because it saves computational time. Shells are curved, thin-walled structures. Ship hulls are typical shell structures because of their curved body that the thickness is relatively small compared to the dimension of the structure. The theory for shells is based on the theory for thin plates, although there is a major behavioural difference for plates and shells subjected to external loading. A plate loaded laterally must be imposed by bending and twisting moments in order for the plate to have static equilibrium. For shells, this is not the case, as membrane stresses can transmit the loading. The membrane stresses are distributed uniformly over the thickness of the shell act parallel to the tangential plane of the middle surface (9).
The two main theories for shell analysis are Reissner-Mindlin theory and Kirchoff-Love theory. Reissner-Mindling is a refinement of Kirchoff-Love, where two additional shear stresses are taken into account. This is used when the thickness is significantly smaller than the length and the width of the structure.
The Kirchoff-Love theory is used in this thesis. In addition to there being no transverse shear deformations, the director remains straight and perpendicular to the mid surface during deformation. (1)

4.1.1 Equilibrium and the Principle of Virtual Work

If a geometry is in equilibrium, the forces does not produce any work.(10) The principle of virtual work represents the work by forces through a virtual displacement. We have equilibrium of internal and external forces if the total virtual work, i.e the sum of the external and internal work is zero

$$\delta W = \delta W_{int} + \delta W_{ext} = 0 \tag{4.1}$$

The internal virtual work is negative, and can be represented as

$$\delta W_{int} = -\int_{\Omega} \mathbf{S}\delta\mathbf{E} d\Omega \tag{4.2}$$

The external virtual work can be described by

$$\delta W_{ext} = \int_{\Omega} \boldsymbol{\rho} \cdot \delta\mathbf{u} d\Omega + \int_{\Gamma} \mathbf{t}_{\Gamma} \cdot \delta\mathbf{u} d\Gamma \tag{4.3}$$

Ω is the physical domain, Γ is the boundary, $\mathbf{S}$ is the Piola Kirchoff stress, $\delta\mathbf{E}$ is the virtual Green-Lagrange strain tensor, $\boldsymbol{\rho}$ is the body force, $\mathbf{t}_{\Gamma}$ is the stress vector at the boundary, and $\delta\mathbf{u}$ is the virtual displacement (1). Virtual work must be fulfilled for any variation of displacements

$$\delta W = \frac{\partial W}{\partial u_r}\delta u_r = 0 \rightarrow \frac{\partial W}{\partial u_r} = 0 \tag{4.4}$$

To solve the nonlinear system, Eq.4.4 is linearized

$$\frac{\partial W}{\partial u_r} + \frac{\partial^2 W}{\partial u_r \partial u_s}\Delta u_s = 0 \tag{4.5}$$

The residual force vector, **R**, comes from taking the derivative of the virtual work with respect to a displacement variable, u_r. (4)

$$R_r = \left(\frac{\partial W_{int}}{\partial u_r} + \frac{\partial W_{ext}}{\partial u_r} \right) = F_r^{int} + F_r^{ext} \tag{4.6}$$

where F_r^{int} and F_r^{ext} are internal and external nodal forces, respectively. The stiffness matrix is found by taking the second derivative of the virtual work

$$K_{rs} = -\left(\frac{\partial^2 W_{int}}{\partial u_r \partial u_s} + \frac{\partial^2 W_{ext}}{\partial u_r \partial u_s} \right) = F_{rs}^{int} + K_{rs}^{ext} \tag{4.7}$$

Lastly, we have the equation system

$$\mathbf{Ku} = \mathbf{R} \tag{4.8}$$

4.2 Isogeometric Analysis

In Isogeometric Analysis(IGA), the basis functions used to represent the geometry are used in analysis to approximate the solution field.
A NURBS-based Kirchoff-Love shell element was developed by Kiendl et al. (**?**). The residual force vector components are represented as

$$R_r = \int_A \left(\mathbf{n} : \frac{\partial \boldsymbol{\varepsilon}}{\partial u_r} + \mathbf{m} : \frac{\partial \boldsymbol{\kappa}}{\partial u_r} \right) dA - \sum_i \int_A \mathbf{P}_i \cdot \frac{\partial \mathbf{u}_i}{\partial u_r} dA - \sum_j \mathbf{F}_j \cdot \frac{\partial \mathbf{u}_j}{\partial u_r}, \tag{4.9}$$

and the stiffness matrix is expressed as

$$K_{rs} = \int_A \left(\frac{\partial \mathbf{n}}{\partial u_s} : \frac{\partial \boldsymbol{\varepsilon}}{\partial u_r} + \mathbf{n} : \frac{\partial^2 \boldsymbol{\varepsilon}}{\partial u_r \partial u_s} + \left(\frac{\partial \mathbf{m}}{\partial u_s} : \frac{\partial \boldsymbol{\kappa}}{\partial u_r} + \mathbf{m} : \frac{\partial^2 \boldsymbol{\kappa}}{\partial u_r \partial u_s} \right) dA + K_{rs}^{ext}. \tag{4.10}$$

n is an internal membrane force, while m is an internal membrane moment. ε represents the strains, and κ is the curvature. **P** and F are area and point loads.

4.2.1 Integration of NURBS surfaces

Integration of NURBS surfaces are performed element-wise using [p+1,q+1] quadrature points. The element stiffness matrix is approximated as the sum of the element stiffness matrix for each Gauss quadrature point, with the corresponding weighs and Jacobian mapping. Then the total stiffness matrix is constructed, and solved for a chosen set of boundary conditions and external forces from Eq. 4.8. The area of an element, represented by knot span indices ij is

$$|A|_{ij} = \int_{A_{ij}} dA_{ij} = \int_{s_{start}}^{s_{end}} \int_{t_{start}}^{t_{end}} J_1 ds dt = \int_{\mathcal{G}} J_1 J_3 d\mathcal{G} \tag{4.11}$$

where s_{start}, s_{end} and t_{start}, t_{end} are the starting and ending points of the element in s- and d-direction in parametric space. The jacobian, J_1 is the mapping from geometry to parameter space, and J_3 is the mapping from parameter space to Gaussian space.

$$J_1 = |\mathbf{A}_1 x \mathbf{A}_2|, \quad J_3 = \frac{\partial s}{partial \xi} \frac{\partial t}{partial \eta}, \tag{4.12}$$

where ξ and η are the paraters in Gaussian space.
The area can be approximated as a sum of all mappings, using n_g quadrature points, and the weights w_l corresponding to the integration points ξ_l, η_l:

$$|A|_{ij} \approx \sum_{l=0}^{n_g} J_1(\xi_l, \eta_l) J_3(\xi_l, \eta_l) w_l. \tag{4.13}$$

4.2.2 Refinement

There are two methods of refining a NURBS surface or curve; knot insertion and order elevation. Both increase the accuracy of the analysis, and both lead to a higher number of control points. Knot insertion divide the surface into smaller parts by adding non-existing knots to the knot span. One control point is added for every knot.
Knots can also be added at existing knots to decrease the continuity at the knot. Order elevation does not change the number of elements, but existing knots are added, to keep the continuity at the knots. Knot insertion is analogous to h-refinement in FEA, as both methods lead to a higher number of elements. the major difference between refinement of NURBS surfaces and refinement in FEA is that the geometrical shape always remains the same in IGA. Order elevation is analogous to p-refinement in FEA.
Local refinement of NURBS surfaces is not possible, because knot insertion extends the whole patch. An alternative to NURBS are T-splines which permits T-junctions. This means the knot does not need to extend the whole patch, thus making local refinement possible. T-splines also allow more control of the control points, thus making it possible to have fewer control points at locations that are not important in an analysis. This is advantageous when it comes to computational effort and time.

Chapter 5

Analysis of Trimmed Elements

Trimmed elements can not be treated as normal, untrimmed elements in Isogeometric Analysis. First of all, the inactive elements should not be considered for the integration of the stiffness matrix. Trimmed elements contribute to the stiffness matrix, but the location of the Gauss quadrature points need to be mapped in some way to represent the actual geometry of the element by accounting for the trimming curve.

What changes during the integration of the stiffness matrix is the area of a knot span ij if the knot span represents a trimmed element and the location and weights of the quadrature points. There are several methods proposed for the mapping of trimmed elements.
Three of these will be discussed in this chapter: NURBS enhanced triangles introduced in Kim et al. (6; 7), Adaptive Gaussian integration procedure (AGIP) proposed by M. Breitenberg (2), and the blending function method presented by Guo et al. (5).

5.1 NURBS Enhanced Triangles

NURBS Enhanced Triangles are a method used for integration of trimmed surfaces. The trimmed elements are divided into triangles and NURBS curved triangles. For the three cases of trimmed elements previously mentioned, the division is shown in Figure 5.1.

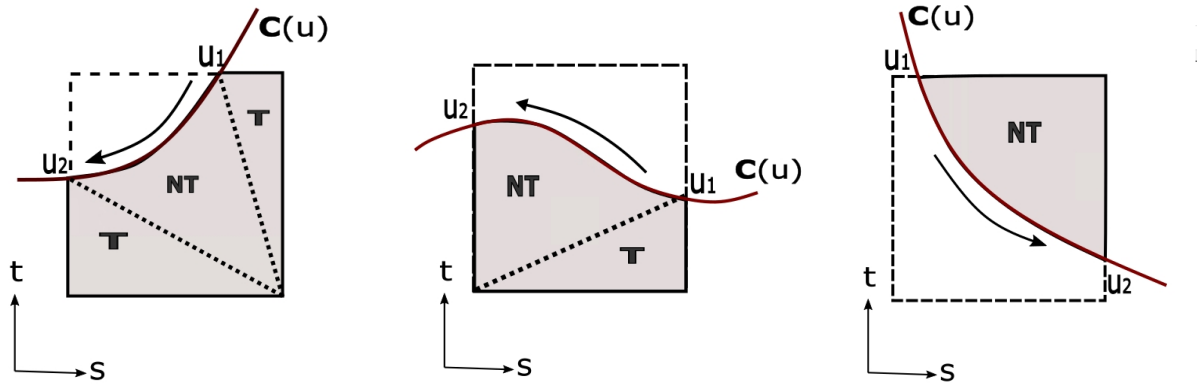

(a) Case 1 (b) Case 2 (c) Case 3

Figure 5.1: Subdivision of elements intro triangles and NURBS curved triangles for the three element cases

5.1.1 Untrimmed quadrilateral elements

The untrimmed elements are normal quadrilateral elements defined by the knot spans $[s_i, s_{i+1}]$ and $[t_j, t_{j+1}]$. Figure 5.2 shows the mapping of an untrimmed element from Gaussian space to parametric space.

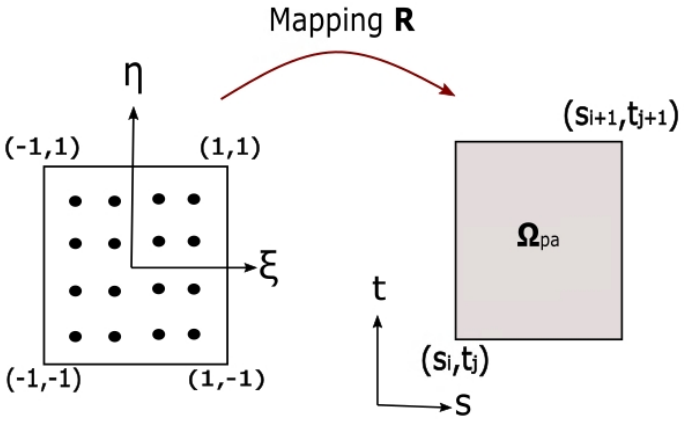

Figure 5.2: Mapping from Gaussian space to Parametric space for untrimmed, quadrilateral elements.

The coordinates in parametric space can be found from the relation:

$$\begin{gathered} \mathbf{R}: \quad \{\xi, \eta\} \rightarrow \{s, t\} \\ \begin{bmatrix} s \\ t \end{bmatrix} = \begin{bmatrix} \frac{s_{i+1}-s_i}{2}(\xi - 1) + s_{i+1} \\ \frac{t_{j+1}-t_j}{2}(\eta - 1) + t_{j+1} \end{bmatrix} \end{gathered} \tag{5.1}$$

Where (ξ, η) are the parameters in Gaussian space. The Jacobian is defined as:

$$\mathbf{J}_R = \begin{bmatrix} \frac{\partial s}{\partial \xi} & \frac{\partial t}{\partial \xi} \\ \frac{\partial s}{\partial \eta} & \frac{\partial t}{\partial \eta} \end{bmatrix} = \begin{bmatrix} \frac{s_{i+1}-s_i}{2} & 0 \\ 0 & \frac{j+1-t_j}{2} \end{bmatrix} \tag{5.2}$$

$$|\mathbf{J}| = |\mathbf{J}_R| \tag{5.3}$$

5.1.2 Normal, Triangular Elements

The subdivided elements which form normal triangles can be integrated using Gauss quadrature points for triangles, and a mapping from triangular Gaussian space to a triangle in parametric space, as shown in figure5.3. The Gauss integration points for triangular elements, $(\xi_{T,l}, \eta_{T,l})$, and their corresponding weights, $W_{T,l}$ can be found as

$$\begin{gathered} \xi_{T,l} = \frac{(1+\xi_i)}{2}, \quad \eta_{T,l} = \frac{(1-\xi_i)(1+\eta_j)}{4}, \quad W_{T,l} = \frac{(1-\xi_i)}{8} w_i w_j, \\ k = 1, 2, ..., n_{int}, \quad i, j = 1, 2, ..., n_g. \end{gathered} \tag{5.4}$$

where ξ_i, η_j are the Gaussian integration points in ξ- and η-direction with w_i and w_j being their corresponding weights.

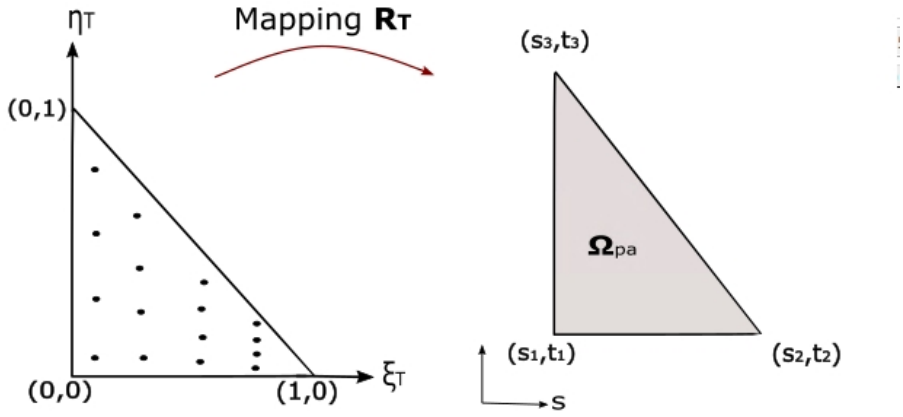

Figure 5.3: Mapping from Gaussian space to Parametric space for normal, triangular elements.

The Parametric coordinates (s,t) for each triangular Gauss point is found by using the coordinates of the vertexes of the triangles.
These can be found as intersection points and vertexes of the quadrilateral element.
For example, the vertices of the triangular sub-element in Figure 5.1 (b) are defined by vertex point 1 and 2 of the original quadrilateral element, and intersection point, u_1.
The mapping from Gauss space to a trinagular domain in parameter space is defined by:

$$\mathbf{R}_T \quad \{\xi_T, \eta_T\} \rightarrow \{s, t\}$$

$$\begin{bmatrix} s \\ t \end{bmatrix} = \begin{bmatrix} (1-\xi_T-\eta_T)s_1 + (\xi_T)s_2 + (\eta_T)s_3 \\ (1-\xi_T-\eta_T)t_1 + (\xi_T)t_2 + (\eta_T)t_3 \end{bmatrix} \tag{5.5}$$

$$\mathbf{J}_{R_T} = \begin{bmatrix} \frac{\partial s}{\partial \xi} & \frac{\partial t}{\partial \xi} \\ \frac{\partial s}{\partial \eta} & \frac{\partial t}{\partial \eta} \end{bmatrix} = \begin{bmatrix} -s_1 + s_2 & -t1 + t_2 \\ -s_1 + s_3 & -t1 + t_3 \end{bmatrix} \tag{5.6}$$

The area of a trimmed element for triangular elements is found by the Jacobian as.

$$|\Omega_{ij}^{(h)}| \approx \sum_{l=1}^{n_g} |J_1(\xi_l, \eta_l)||J_{R_T}(\xi_{T,l}, \eta_{T,l})|W_{T,l} \tag{5.7}$$

Where J_1 is defined in Eq.4.12, and n_g are the number of integration points.

5.1.3 NURBS enhanced triangles

NURBS enhances triangles uses several mappings from Gaussian space to parametric space.
First, the quadrilateral Gaussian space is mapped to a quadrature space Ψ_e which ranges from [0,1] in z-direction and $[u_1, u_2]$ in u-direction. u_1 and u_2 are the intersection points between the trimming trimming curve and the element where

$$0 \leq u_1 < u_2 \leq 1 \tag{5.8}$$

.
This mapping is shown in Figure 5.4.

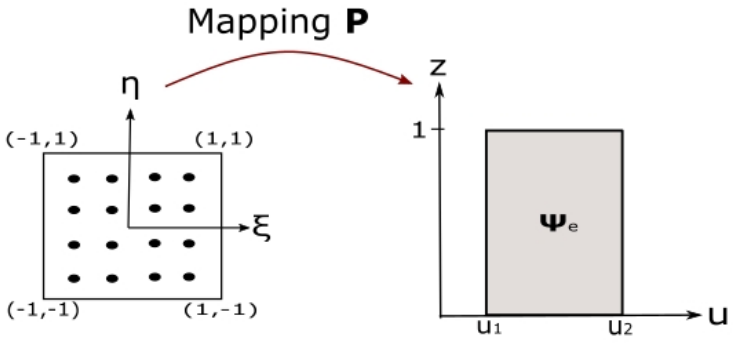

Figure 5.4: Mapping from Gaussian space to rectangular space with boundaries $z = [0,1]$ and $u = [u_1, u_2]$.

The mapping P is defined as:

$$\mathbf{P}: \quad \{\xi, \eta\} \rightarrow \{u, z\}$$

$$\begin{bmatrix} u \\ z \end{bmatrix} = \begin{bmatrix} \frac{\xi}{2}(u_2 - u_1) + \frac{1}{2}(u_2 + u_1 \\ \frac{\eta}{2} + \frac{1}{2} \end{bmatrix} \tag{5.9}$$

And the Jacobian of the mapping P is:

$$\mathbf{J}_P = \begin{bmatrix} \frac{\partial u}{\partial \xi} & \frac{\partial z}{\partial \xi} \\ \frac{\partial u}{\partial \eta} & \frac{\partial z}{\partial \eta} \end{bmatrix} = \begin{bmatrix} \frac{u_2 - u_1}{2} & 0 \\ 0 & \frac{1}{2} \end{bmatrix} \tag{5.10}$$

The second mapping is from the quadrilateral space Ψ_e to a triangular space T_e with vertices (0,1), (1,0) and (0,0). In addition the domain T_e has a NURBS curve $\phi(u)$ which intersects T_e at vertices (0,0) and (1,0).

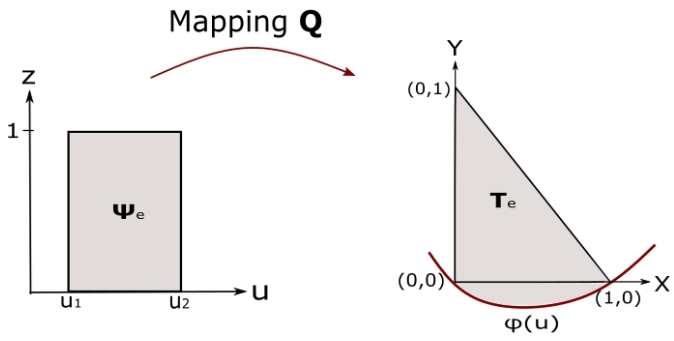

Figure 5.5: Mapping from rectangular space to triangular domain defined by vertices (0,1), (0,0) and (1,0) and a NURBS curve ϕ(u)

The parameters of T_e are (X,Y), which can be found by:

$$\mathbf{Q}: \quad \{u,z\} \rightarrow \{X,Y\}$$

$$\begin{bmatrix} X \\ Y \end{bmatrix} = \begin{bmatrix} \phi_X(u)(1-z) \\ \phi_Y(u)(1-z)+z \end{bmatrix} \tag{5.11}$$

How to determine $\phi(u)$ will be discussed below. The Jabobian of the mapping $\mathbf{Q}$ is:

$$\mathbf{J}_Q = \begin{bmatrix} \frac{\partial X}{\partial u} & \frac{\partial Y}{\partial u} \\ \frac{\partial X}{\partial z} & \frac{\partial Y}{\partial z} \end{bmatrix} = \begin{bmatrix} \frac{\partial \phi_X(u)}{\partial u}(1-z) & \frac{\partial \phi_Y(u)}{\partial u}(1-z) \\ -\phi_X(u) & -\phi_Y(u)+1 \end{bmatrix} \tag{5.12}$$

The last mapping is the mapping from the triangular space T_e to the triangular sub-element in parametric space, Ω_{pa}, shown in figure 5.6.

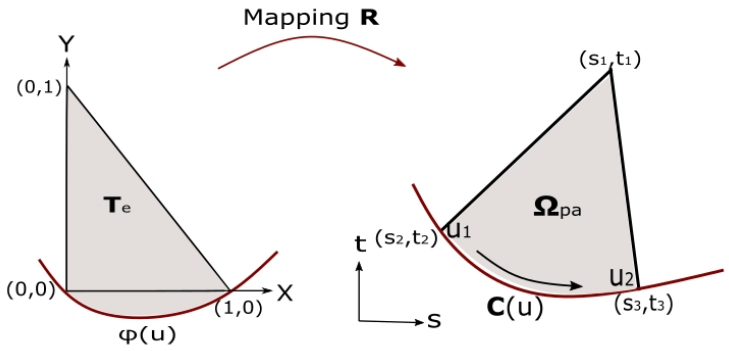

Figure 5.6: Mapping from triangular domain $\mathbf{T}_e$ to parametric space $\mathbf{\Omega}_{pa}$.

The coordinates (s_2,t_2) and (s_3,t_3) are found by the intersection points, u_1 and u_2.

$$(s_2,t_2) = \mathbf{C}(u_1), \quad (s_3,t_3) = \mathbf{C}(u_2), \tag{5.13}$$

while (s_1,t_1) lies on one of the vertex points of the original element. Them, the parametric coordinates s and t can be expressed as:

$$\mathbf{R}: \quad \{X,Y\} \rightarrow \{s,t\}$$

$$\begin{bmatrix} s \\ t \end{bmatrix} = \begin{bmatrix} (Y)s_1 + (1-X-Y)s_2 + (X)s_3 \\ (Y)t_1 + (1-X-Y)t_2 + (X)t_3 \end{bmatrix} \tag{5.14}$$

And the Jacobian of the mapping $\mathbf{R}$ is found by:

$$\mathbf{J}_R = \begin{bmatrix} \frac{\partial s}{\partial X} & \frac{\partial t}{\partial X} \\ \frac{\partial s}{\partial Y} & \frac{\partial t}{\partial Y} \end{bmatrix} = \begin{bmatrix} -s_2+s_3 & -t_2+t_3 \\ s_1-s_2 & t_1-t2 \end{bmatrix} \tag{5.15}$$

The total mapping is the product of all determinants of the separate mappings.

$$|\mathbf{J}| = |\mathbf{J}_P||\mathbf{J}_Q||\mathbf{J}_R|, \tag{5.16}$$

and so the area of the trimmed element can be described as

$$|\Omega_{ij}^{(h)}| \approx \sum_{l=1}^{n_g} |J_1||J(\xi_l,\eta_l|W_l, \quad W_l = w_i w_j \tag{5.17}$$

where w_i and w_j are the weight corresponding to the quadrature points ξ_l and η_l respectively. The NURBS curve $\phi(u)$ can be found from the relation

$$\boldsymbol{\phi}(u) = \begin{bmatrix} \phi_X(u) \\ \phi_Y(u) \end{bmatrix} = [\mathbf{A}_1]^{-1} \left(\begin{bmatrix} C_s(u) \\ C_t(u) \end{bmatrix} - [\mathbf{A}_2] \right), \tag{5.18}$$

Where $[\mathbf{A}_1]$ is a 2x2 matrix and $[\mathbf{A}_2]$ is a 2x1 matrix.

The derivative can then be expressed as:

$$\begin{bmatrix} \frac{\partial \phi_X(u)}{\partial u} \\ \frac{\partial \phi_Y(u)}{\partial u} \end{bmatrix} = [\mathbf{A}_1]^{-1} \begin{bmatrix} \frac{\partial C_{,s}(u)}{\partial u} \\ \frac{\partial C_{,t}(u)}{\partial u} \end{bmatrix} \tag{5.19}$$

The matrices $[\mathbf{A}_1]$ and $[\mathbf{A}_2]$ are found from the relation:

$$\begin{bmatrix} s \\ t \end{bmatrix} = [\mathbf{A}_1] \begin{bmatrix} X \\ Y \end{bmatrix} + [\mathbf{A}_2] \tag{5.20}$$

Rearranging Equation 5.15 gives an expression for the two A-matrices:

$$\begin{bmatrix} s \\ t \end{bmatrix} = \begin{bmatrix} s_3 - s_2 & s_1 - s_2 \\ t_3 - t_2 & t_1 - t_2 \end{bmatrix} \begin{bmatrix} X \\ Y \end{bmatrix} + \begin{bmatrix} s_2 \\ t_2 \end{bmatrix} \tag{5.21}$$

5.2 Adaptive Gaussian Integration Procedure

The idea behind Adaptive Gaussian Integration Procedure is to reconstruct a trimmed element inside a Gaussian space, $\mathcal{G}_A$, and distribute the Gaussian quadrature points to the untrimmed, constructed surface.
For a trimmed element, the curve is scaled and shifted to fit the Gaussian space [-1,1], and rotated so that only the height, $\mathcal{G}_H^A$ varies with respect to ξ, as shown in Figure 5.7

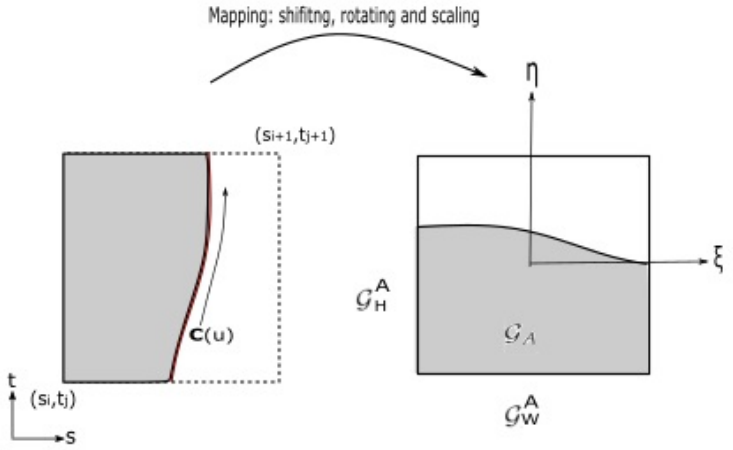

Figure 5.7: Mapping of trimmed element from parameter space to Adaptive Gaussian space

The linear mapping from parametric space to Gaussian space is given by

$$J = |\frac{\partial s}{\partial \xi}\frac{\partial t}{\partial \eta}|, \tag{5.22}$$

when the rotation is 0○ or 180○, and

$$J = |\frac{\partial s}{\partial \eta}\frac{\partial t}{\partial \xi}|, \tag{5.23}$$

when the rotation is 90○ or 270○.
The rotated, shifted and scaled curve in Gaussian space is used to create a surface, $\hat{\mathbf{S}}(\xi,\eta)$.
The surface will be the basis for a set of quadrature points, (ξ_l^A,η_l^A), distributed over the untrimmed surface in the Adaptive Gaussian space. The Adaptive quadrature points can be found from:

$$(\xi_l^A,\eta_l^A) = \hat{S}(\xi_l,\eta_l), \quad l = 1,2,...,n_g, \tag{5.24}$$

where n_g are the number of quadrature points. the adaptive quadrature weights are given as

$$w_l^A = \tilde{J}(\xi,\eta)w_l, \tag{5.25}$$

where $\tilde{J}$ represents the mapping of the adaptive Gaussian space, similar to Eq.5.23. Using n_g quadrature points, the area of a trimmed element can be computed as

$$|\Omega_{ij}^{(h)} \approx \sum_{l=1}^{n_g} J_1(\hat{\xi}_l^A,\hat{\eta}_l^A)J_2(\hat{\xi}_l^A,\hat{\eta}_l^A)w_l^A \tag{5.26}$$

J_1 is the mapping from physicaL space to parameter space, defined in Eq.4.12
To create the surface $\hat{\mathbf{S}}$, C^0 continuity is imposed on the curve at intersection points, u_1 and u_2, of each trimmed element.
Figure 5.8 (a) shows a trimmed element in parameter space with trimming curve, $\mathbf{C}(u)$. The curve is then scaled to u=[-1,1] to fit the Gaussian space.
There is no need for rotation or fitting for this particular element. Figure 5.8 (b) shows the constructed surface in Gaussian space.

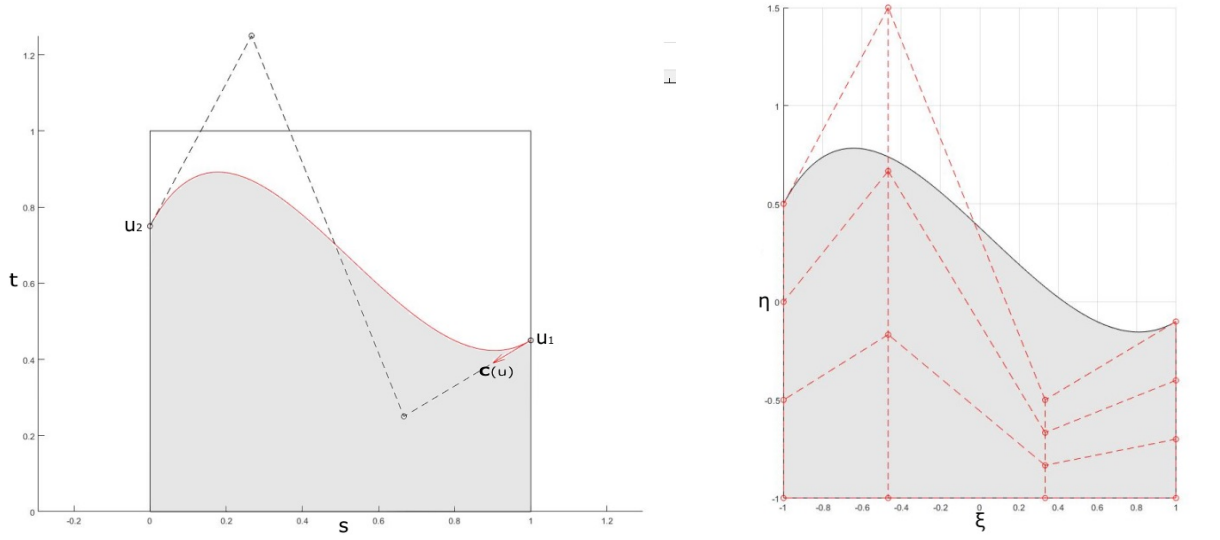

(a) Trimmed element in parametric space (b) Untrimmed surface in Gaussian space

Figure 5.8: Construction of an untrimmed surface from the mapping of a trimming curve

The location of the adaptive Gaussian quadrature points from found by Eq.5.24 are shown in Figure 5.9 (a). These integration points are then mapped back to the parameter space and used for integration of the stiffness matrix. The integration points in parameter space are shown in 5.9 (b).

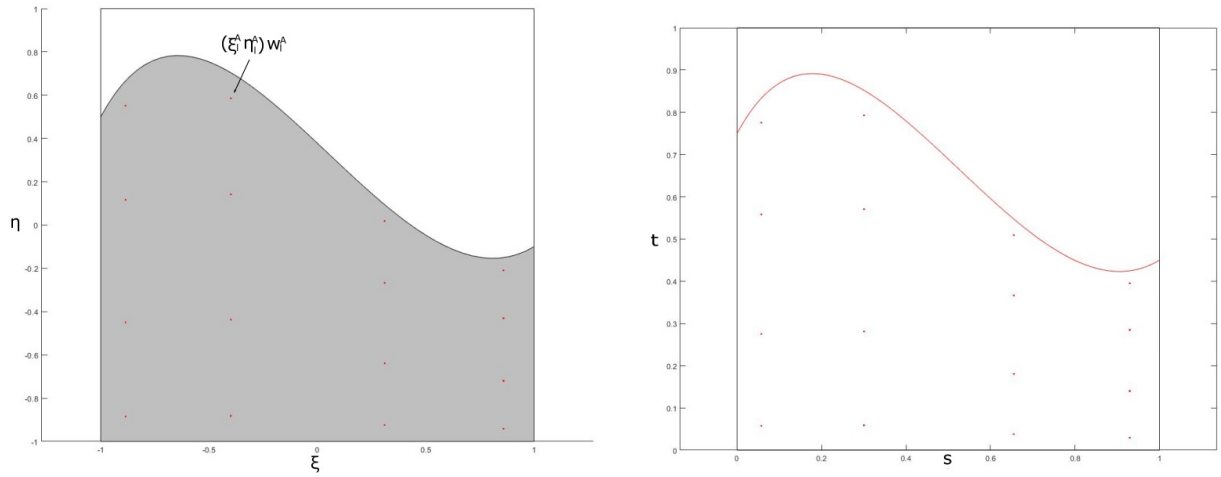

(a) Gaussian space (b) Parameter space

Figure 5.9: Location of integration points for analysis

All trimmed elements that are valid for analysis can be represented by an adaptive Gaussian surface by shifting, scaling and/or rotation of the trimming curve segments with C^0 continuity at intersection points. Figure 3.11 shows a trimmed element with rotation of trimming curve 270∘.

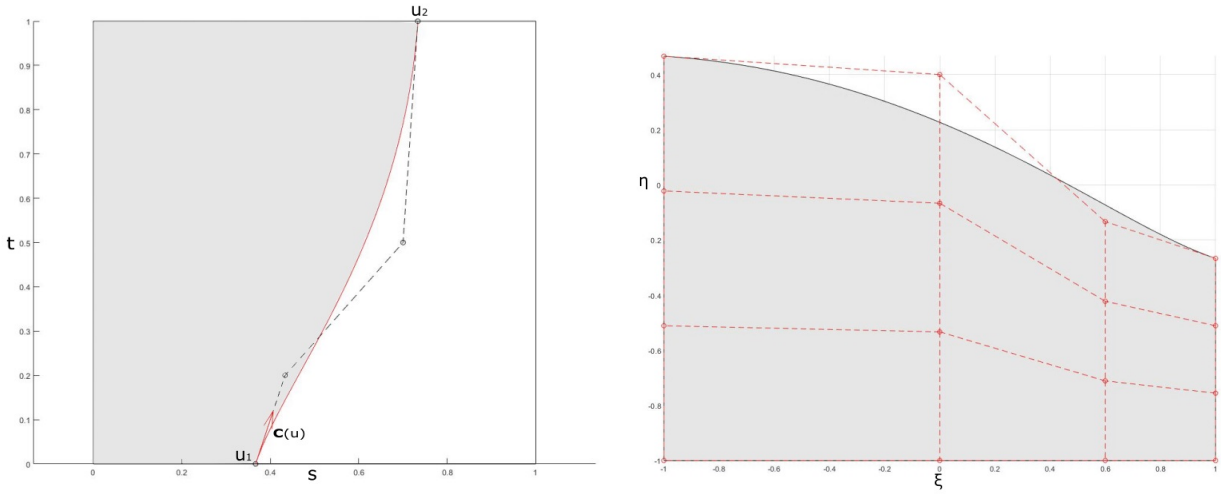

(a) Trimmed element in Parameter space (b) Untrimmed, rotated and scaled surface

Figure 5.10: Scaling and rotation of trimming curve into Gaussian space to construct adaptive Gaussian surface

5.3 The Blending Function Method

The blending function method aims to reconstruct the material region of trimmed elements by dividing the trimming curves at all intersection points, thus giving each trimmed element a separate part of the trimming curve.
The method uses two categories of mapping: Mapping of quadrilateral trimmed elements, and mapping of triangular trimmed elements. These mappings will be discussed further below. Further, any trimmed element which does not represent a triangular or quadrilateral geometry, can be subdivided in various ways until it does.
There are two important aspects to this method, the first being that all curves must be C^0 continuous at all intersection points. This is done to divide the trimming curves into curve segments.
The second aspect is that any curve segments with internal C^0 knots must be subdivided at the location of the knot.
The area of a trimmed element segment used for integration of the element stiffness matrix is found by

$$|\Omega_{ij}^{(h)}| \approx \sum_{l=1}^{n_g} |J_1(\xi_l,\eta_l)||J_R(\xi_l,\eta_l)|w_l \tag{5.27}$$

where w_l are the quadrature weight corresponding to each quadrature integration point, (ξ_l,η_l), and n_g are the number of integration points. How to find the mapping, J_R, for various element cases will be described in detail in this section.

5.3.1 Quadrilateral trimmed elements

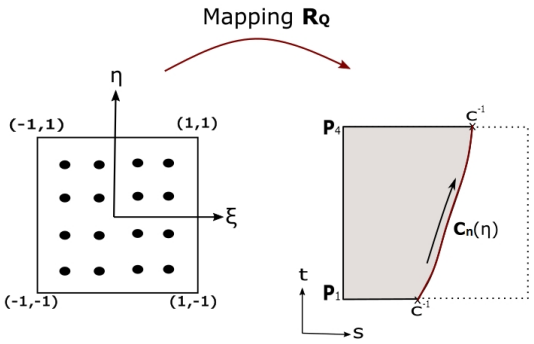

Figure 5.11: Mapping of quadrilateral elements from gauss space to parametric space

Figure 5.11 shows the mapping, $\mathbf{R}_Q$ from Gaussian space to parametric space for a trimmed quadrilateral element. $\mathbf{C}_n(\eta)$ is the trimming curve segment which is parametrized with respect to η=[-1,1]. $\mathbf{P}_1$ and $\mathbf{P}_1$ are vertex points of the element. The mapping is given by:

$$\begin{gathered}\mathbf{R}_Q: \quad \{\xi,\eta\} \rightarrow \{s,t\} \\ \begin{bmatrix} s \\ t \end{bmatrix} = \tfrac{1}{4}((1-\xi)(1-\eta)\mathbf{P}_1 + (1-\xi)(1+\eta)\mathbf{P}_4) + \tfrac{1}{2}\mathbf{C}_n(\eta)(1+\xi),\end{gathered} \tag{5.28}$$

Similar mapping exists for various rotation of the element. This means all quadrilateral trimmed elements can be mapped using this method, as long as the conditions for a valid element cases are met.
The other three quadrilateral elements with a rotation of 90○, 180○ and 270○ are shown in Figure 5.12.

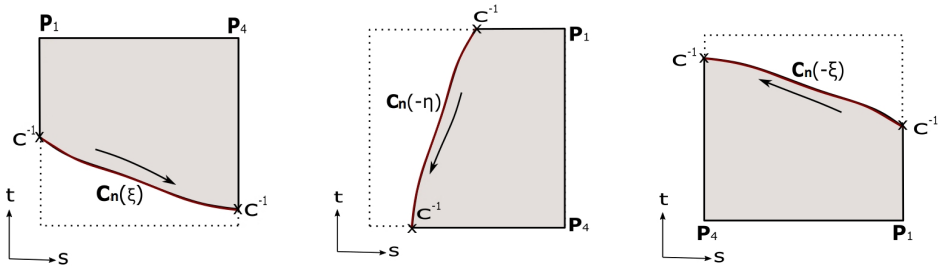

(a) Rotation 90° (b) Rotation 180° (c) Rotation 270°

Figure 5.12: Rotation of quadrilateral trimmed elements for mapping

The various rotations require different parametrizations of the trimming curve segments, as can be seen in Figure 5.12. The mapping for the different rotations are given below.

$$90°\,Rotation: \begin{bmatrix} s \\ t \end{bmatrix} = \frac{1}{4}((1-\xi)(1+\eta)\mathbf{P}_1 + (1+\xi)(1+\eta)\mathbf{P}_4) + \frac{1}{2}\mathbf{C}_n(\xi)(1-\eta), \tag{5.29}$$

$$180°\,Rotation: \begin{bmatrix} s \\ t \end{bmatrix} = \frac{1}{4}((1+\xi)(1+\eta)\mathbf{P}_1 + (1+\xi)(1-\eta)\mathbf{P}_4) + \frac{1}{2}\mathbf{C}_n(-\eta)(1-\xi), \tag{5.30}$$

$$270°\,Rotation: \begin{bmatrix} s \\ t \end{bmatrix} = \frac{1}{4}((1+\xi)(1-\eta)\mathbf{P}_1 + (1-\xi)(1-\eta)\mathbf{P}_4) + \frac{1}{2}\mathbf{C}_n(-\xi)(1+\eta), \tag{5.31}$$

The Jacobian for quadrilateral trimmed elements is given by:

$$\mathbf{J}_R = \begin{bmatrix} \frac{\partial s}{\partial \xi} & \frac{\partial t}{\partial \xi} \\ \frac{\partial s}{\partial \eta} & \frac{\partial t}{\partial \eta} \end{bmatrix} \tag{5.32}$$

5.3.2 Triangular trimmed elements

The mapping for triangular trimmed elements are based on the one for quadrilateral, where two corners of the active domain are joined together. The mapping from Gaussian space to parametric space for a triangular trimmed element, $\mathbf{R}_T$ is shown in figure 5.13.

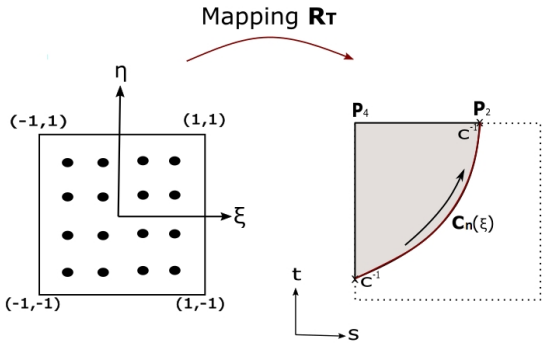

Figure 5.13: Mapping of triangular elements from Gauss space to parametric space

The trimming curve segment is parametrized with respect to ξ=[-1,1], and the mapping can be found by the relation:

$$\begin{gathered}\mathbf{R}_T: \quad \{\xi,\eta\} \rightarrow \{s,t\} \\ \begin{bmatrix} s \\ t \end{bmatrix} = \tfrac{1}{4}((1+\xi)(1+\eta)\mathbf{P}_2 + (1-\xi)(1+\eta)\mathbf{P}_4) + \tfrac{1}{2}\mathbf{C}_n(\xi)(1-\eta),\end{gathered} \tag{5.33}$$

Following the procedure of the quadrilateral trimmed elements, the element can be rotated to depict all possible and valid cases of trimmed triangular elements.

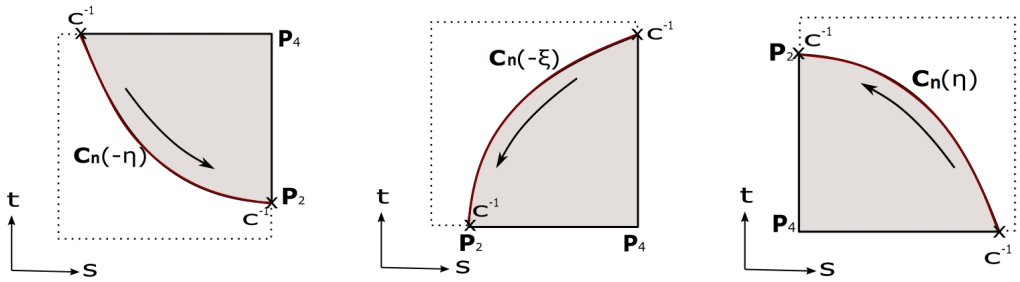

(a) Rotation 90° (b) Rotation 180° (c) Rotation 270°

Figure 5.14: Rotation of triangular trimmed elements for mapping

Figure 5.14 shows the triangular element rotated 90○, 180○ and 170○, with the respective parametrizations of the trimming curve segments. The mapping, $\mathbf{R}_T$ for the three cases are:

$$90^\circ Rotation: \begin{bmatrix} s \\ t \end{bmatrix} = \frac{1}{4}((1+\xi)(1-\eta)\mathbf{P}_2 + (1+\xi)(1+\eta)\mathbf{P}_4) + \frac{1}{2}\mathbf{C}_n(-\eta)(1-\xi), \tag{5.34}$$

$$180^\circ Rotation: \begin{bmatrix} s \\ t \end{bmatrix} = \frac{1}{4}((1-\xi)(1-\eta)\mathbf{P}_2 + (1+\xi)(1-\eta)\mathbf{P}_4) + \frac{1}{2}\mathbf{C}_n(-\xi)(1+\eta), \tag{5.35}$$

$$270^\circ Rotation: \begin{bmatrix} s \\ t \end{bmatrix} = \frac{1}{4}((1-\xi)(1+\eta)\mathbf{P}_2 + (1-\xi)(1-\eta)\mathbf{P}_4) + \frac{1}{2}\mathbf{C}_n(\eta)(1+\xi), \tag{5.36}$$

The Jacobian for trimmed triangular elements is found the same way as for trimmed quadrilateral elements.

$$\mathbf{J}_R = \begin{bmatrix} \frac{\partial s}{\partial \xi} & \frac{\partial t}{\partial \xi} \\ \frac{\partial s}{\partial \eta} & \frac{\partial t}{\partial \eta} \end{bmatrix} \tag{5.37}$$

5.3.3 Subdivision of trimmed elements

There are two cases where subdivision is necessary when applying the blending function method to analysis of trimmed elements: If the element is classified as case 1, or if there are internal C^0 knots inside a trimming curve segment.
Elements of case 1 have three active vertex points and one inactive. This means the shape of the domain does not represent a quadrilateral geometry, nor a triangular. Figure 5.15 is an example of this element type, where vertex point 1 is inactive.

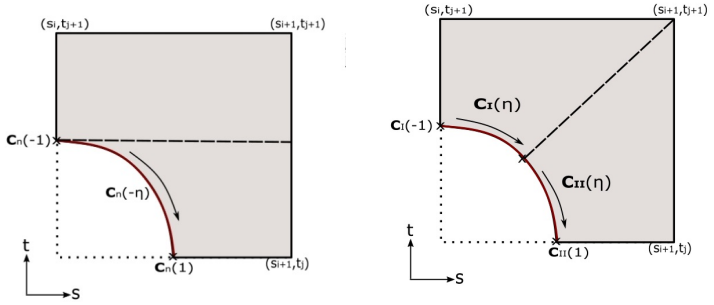

(a) Horizontal subdivision (b) Diagonal subdivision

Figure 5.15: Subdivision of elements classified as case 1.

There are several ways to subdivide this type of element. One method is to subdivide horizontally or vertically at the beginning or the end of the trimming segment, depending on the location. This is shown in Figure 5.15 (a). Another method is shown in 5.15 (b), where the element is subdivided diagonally from the middle of the trimming curve segment. The advantage to diagonal subdivision is that the two sub domains will be approximately equal in area, meaning the Gauss quadrature points will be evenly spaces. However, this requires further division of the trimming curve segments.
As shown in 5.15 (b), the curve segment $\mathbf{C}_n$ is divided into $\mathbf{C}_I$ and $\mathbf{C}_{II}$. For simplicity, horizontal subdivision will be used in this thesis.
For the case of internal C^0 knots, the elements must be subdivided at this location. Figure 5.16 shows a quadrilateral and a triangular trimmed element with internal C^0 knots. The quadrilateral element is subdivided into two quadrilateral elements.
In the case of additional inner C^0 knots, more subdivisions into quadrilaterals will be performed. For the case of triangular element, subdivision leads to one triangular element, and one quadrilateral. Again, multiple C^0 knots produces multiple quadrilaterals.

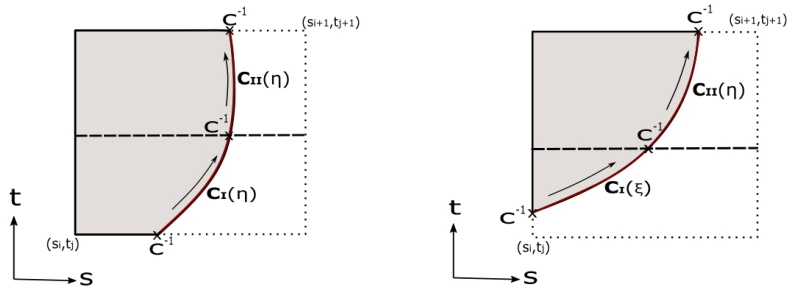

(a) Quadrilateral trimmed elements (b) Triangular trimmed elements

Figure 5.16: Subdivision of elements because of inner C^0 knots

5.4 Conditions for the integration domain

Integration of the element stiffness matrix for the trimmed element cases described in Chapter 3 can be performed using either mapping presented above.
As mentioned, there are some conditions which need to be fulfilled in order for the integration domain to be suitable for analysis.

1. Undercuts can only occur in one direction, s or t.
2. No closed curves inside an element
3. There can only be one trimming curve per element
4. The trimmed element must be represented by one of the three cases, meaning the trimming curve must cross at least one of the element vertex points.

The trimmed surface in Figure 3.10 (a) has undercuts in both s- and t-direction.
To illustrate the problem with this type of trimmed elements, the Gauss quadrature points are plotted and shown in Figure 5.17.
At the location of the second undercut, the element becomes unavailable for analysis because the integration points appear outside of the trimmed domain.

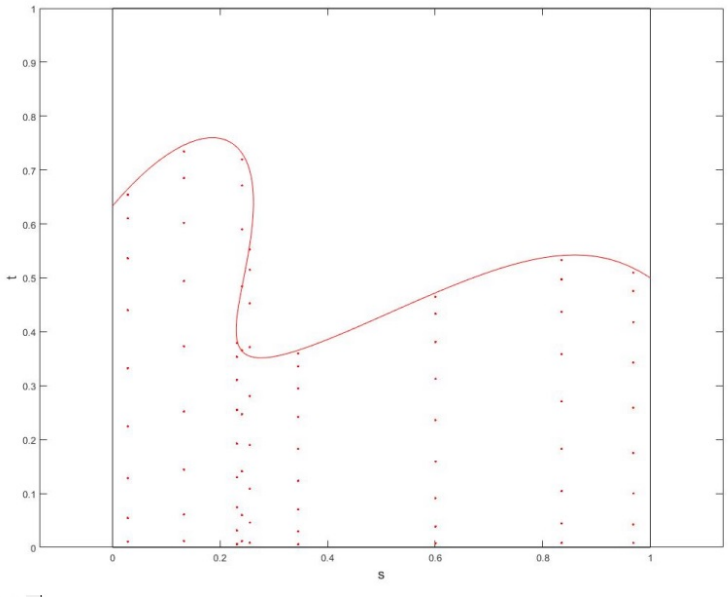

Figure 5.17: Integration points for an element with undercuts in s- and t-direction.

5.5 Determination of active control points

Even though an element is classified as inactive, meaning it lies outside of the trimmed domain, it might contain active control points. For analysis of trimmed surfaces it is important to identify inactive control points and exclude their contribution in the relation

$$\mathbf{Ku} = \mathbf{R} \tag{5.38}$$

Figure 5.18 shows a trimmed surface in physical space with control points and a control point net. There are 11 control points in each direction, x and y.

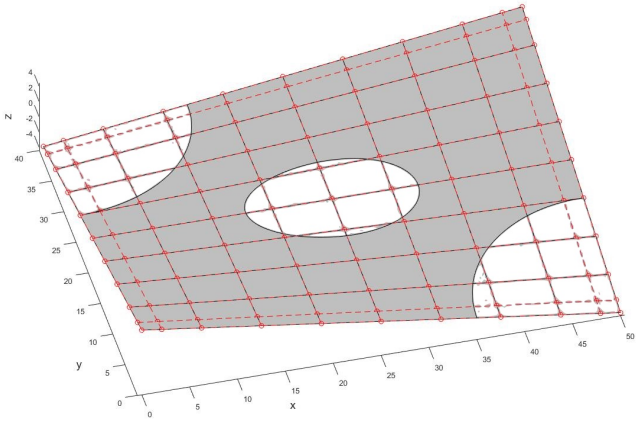

Figure 5.18: Trimmed surface in physical space.

Figure 5.19 shows the surface in parametric space, with the knot spans marked s_i, t_j. The knot vectors S, and T each consists of 15 knots. The polynomial degrees are p=q=3. The indexes 1-3 and 13-15 are zero-knots spans. The remaining index spaces i,j represent trimmed, untrimmed or inactive patches. There are six inactive patches, three at the upper right corner, and three at the lower left corner. The trimmed elements has influence over the control points (i-p+b,j-q+c), where b=1,2,..,p and c=1,2,..,q. Because of this only the three rightmost control points in the lower corner and the three leftmost control points in the upper corner are inactive.

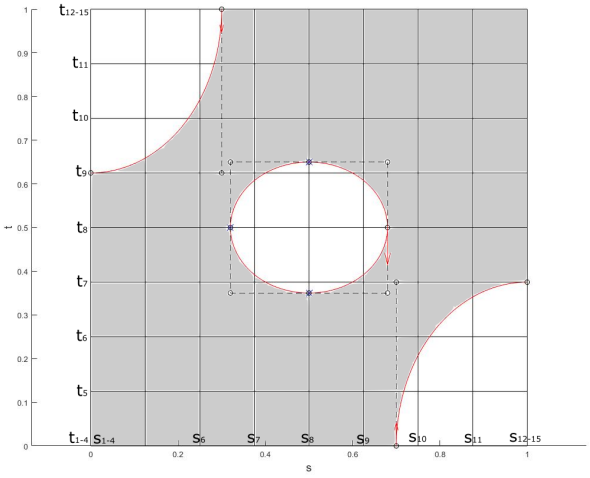

Figure 5.19: Trimmed surface in physical space.

The displacements of the inactive control points, $[d_{10,1}\ d_{11,1}\ d_{11,2}\ d_{1,10}\ d_{1,11}\ d_{2,11}]$ are set to zero for the analysis.

5.6 Comparison of the mapping methods

Apart from the conditions the trimmed elements must satisfy for analysis, some of the mapping methods also have additional conditions to fulfill.
As mentioned, the adaptive Gaussian integration procedure requires C^0 continuity of the trimming curve at all intersection points. This requires, in most cases, a refinement of the trimming curve at this location.
The blending function method requires the trimming curve to be fully divided into segments by imposing C^-1 continuity at the intersection points. In addition, the element must be subdivided in the event of any internal $C0$ knots.
The trimmed surface in Figure 5.19 har three trimming curves. For the blending function method, all three curves are divided into smaller segments, which can be seen in figure 5.20.

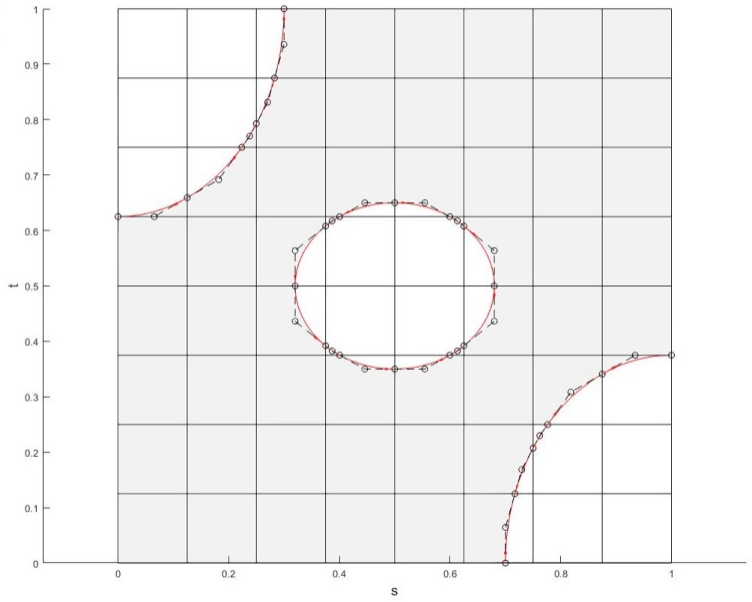

Figure 5.20: Refinement of trimming curves by imposing C^-1 continuity at intersection points.

The NURBS enhanced triangles mapping requires no refinement of the trimming curves, which can be advantageous in terms of computational time. The adaptive Gaussian integration procedure holds and advantage to the other two, in that it requires less subdivision of elements.
Subdivision of the NURBS enhanced triangles are required for elements classified as both case 1 and case 2. How the elements are subdivided is determined based on which vertex points are active, which can lead to some sub-section triangles being represented by a much smaller area than the rest of the elements. For the blending function method subdivision is only required for elements of case 1, but if there are inner C^0 knots, element cases 2 and 3 might also be subdivided.
Subdivision requires more computational time, and gives a more uneven distribution of quadrature points. The trimmed surface from Figure 5.20 is used to show the distribution of integration points using the three mapping methods discussed. Figure 5.21, 5.22 and 5.23 shown the quadrature points for the blending function method, the NURBS enhanced triangles method and the adaptive Gaussian integration procedure, respectively.

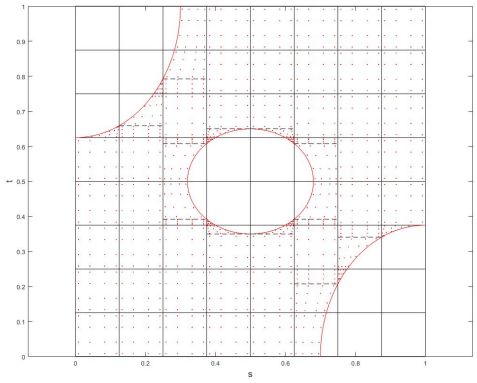

Figure 5.21: Integration points using the blending function method

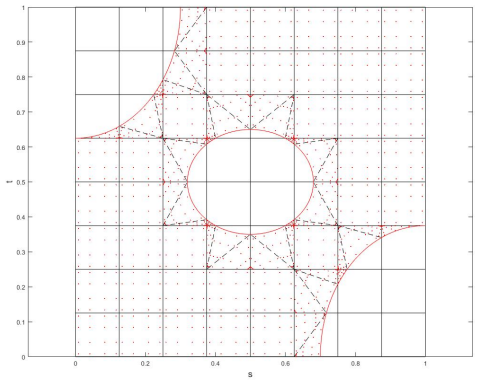

Figure 5.22: Integration points using the NURBS enhanced triangles method.

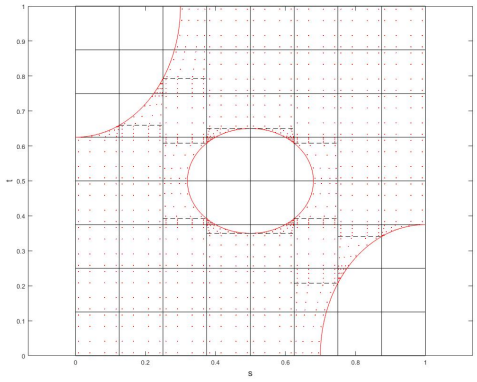

Figure 5.23: Integration points using the adaptive Gaussian integration procedure.

Chapter 6

Structural Analysis of Ship Hulls

Computer simulations are often used in ship design, using mathematical equations to define displacements and stresses on the different parts of the hull. There are many different aspects to analyzing ships. Hydrodynamic analysis is important for the performance of the ship in water, wrt. speed, stability and safety among other factors. Buckling-, strength- and fracture- analysis are also crucial for ships. Ship hulls are exposed to a number of loads in addition to the weight of the cargo and the structure. The water creates a pressure on the bilge of the hull, which depend on the waves. Wind forces are another environmental load, which can affect the stability of the ship hull. Computational fluid dynamics simulations are important when it comes to propulsion design, as for example corrosion is important to avoid. CFD can also be used in hull design, to minimize drag forces.

6.1 Analysis using FEA

The finite element method (FEM) is common practice for analyzing ship hulls. Often, the geometry is created in CAD and imported into a computer program which implements the theory behind FEM for analysis. FEA divides the structure into small elements, and in doing so approximates the original geometry. The collection of elements which make up the structure is called a mesh- Refinement in the form of a finer mesh will improve the quality of the result. Mesh convergence studies are often performed, in which the number of elements are doubled for each analysis, until a converged solution has been reached. The use of FE computer programs helps make analysis of complex structures faster, simpler and more accurate. It also makes it easy to make changes to the geometry and simulate various loading cases, making it possible to find a more optimized model.

6.2 Ship Hull Dimensioning

Basic dimensioning of ships is based on guidelines and knowledge from experience. Solutions obtained from analysis and model testing help build on this knowledge. The finite element method allows for more detailed structural analysis. Classification societies provide some guidelines to the creation of models, and whether or not simplifications can be made. Structurally, a ship can be seen as beam with varying mass and stresses which cause bending and torsion. There are requirements developed for ship building which defines certain dimensions based on loading conditions. This includes the thickness of the shell and other components such as girders and stiffeners. These guidelines and requirements form the basis for the dimensioning of the ship hull. After the main dimensions have been layed out, analysis, often using FEM, can be performed to determine the remaining dimension. A sufficient analysis is crucial to determine whether the ship will be able to withstand the expected stresses and forces it will be subjected to during its lifetime.

6.3 Global and Local Models

An optimal shape of the ship hull is important for the stability, speed, resistance and many other aspects. Figure 6.1 shows an example of a ship hull created in Rhino

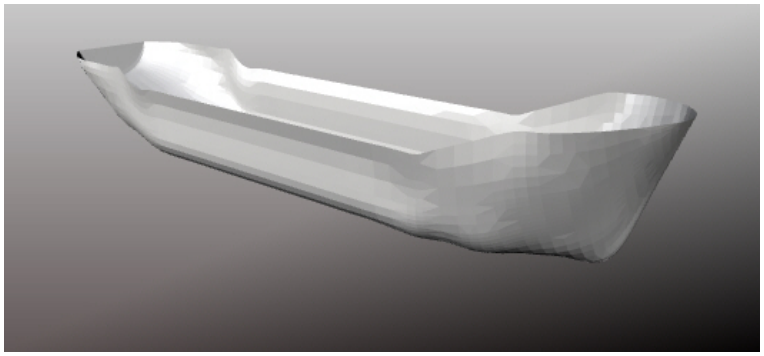

Figure 6.1: Ship hull created in Rhino

Line drawings are often used for designing the shape of the hull. A grid which shows longitudinal lines and water lines is the basis for such drawings. One plane shows the profile of the ship, and the lines in longitudinal direction. The half breath plan shows the lines of the ship from above/below, and the body plan shows the cross section.The line drawings used to create the ship hull are shown in Figure 6.2

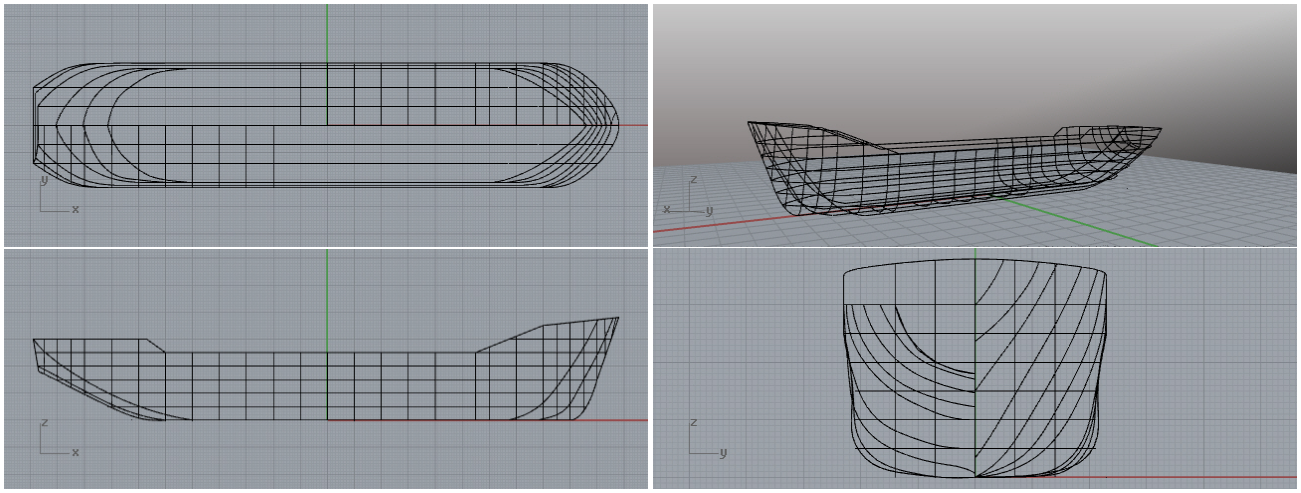

Figure 6.2: Top left: Profile. Top right: Perspective. Bottom left: half breath plan. Bottom right: body plan

Ship are composed of a number of components which make up the entire hull. The entire ship, containing all parts of the structure is called a global model. When analyzing global models, division into smaller parts is usually done in a large scale. Small components such as stiffeners and girders are not analyzed separately, but included in the stiffness of the larger components. The overall performance of the ship hull is what is investigated during the global analysis.
Local model divides the ship further into smaller parts. All parts of the hull is analyzed for during local analysis. This allows for precise stress analysis. Local models are analyzed based on displacement from neighbouring components.

6.4 Isogeometric Trimmed Elements used for Ship Hull Analysis

Isogeometric analysis performs analysis on an exact geometry description, unlike FEA, where the geometry is approximated. Because of this IGA should hold an advantage to classical FEA programs, in reaching a more accurate solution faster. Isogeometric analysis of trimmed structures allow for trimming in CAD, unlike conventional IGA. A trimmed surface representing a local part of a ship hull will be analyzed using both FEA and IGA. FEA models with very fine mesh will be used as a reference solution. figure 6.3 shows various components of a ship hull

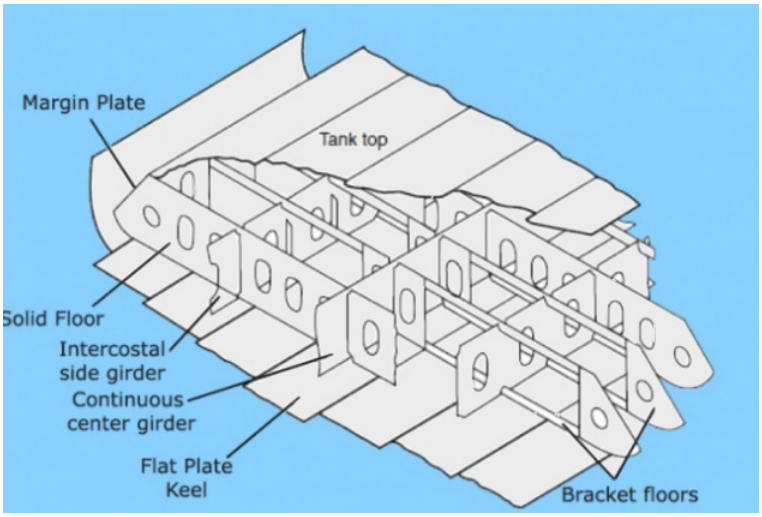

Figure 6.3: Part of a Ship hull

As seen from the figure, a lot of the parts consist of plates with holes. an important aspect to analysis of ship holes is therefore an accurate analysis of these type of components.

6.5 Analysis of A Plate With a Hole

A geometry represents a quarter of a plate with a hole in the middle which will be subjected to a pressure load along the vertical edges. The plate can be modelled as a quarter plate because of symmetry. The quarter plate is therefore a local model of another local model.
The boundary conditions are imposed at the edges where the local model is connected to the plate. The loading is applied along the vertical edge, and has a magnitude of 20 [MPa]. The direction of the loading is in the negative x-direction.
All four local parts will have the same results for stress and displacements. The Trimmed surface created in Rhino is shown in Figure 6.4.

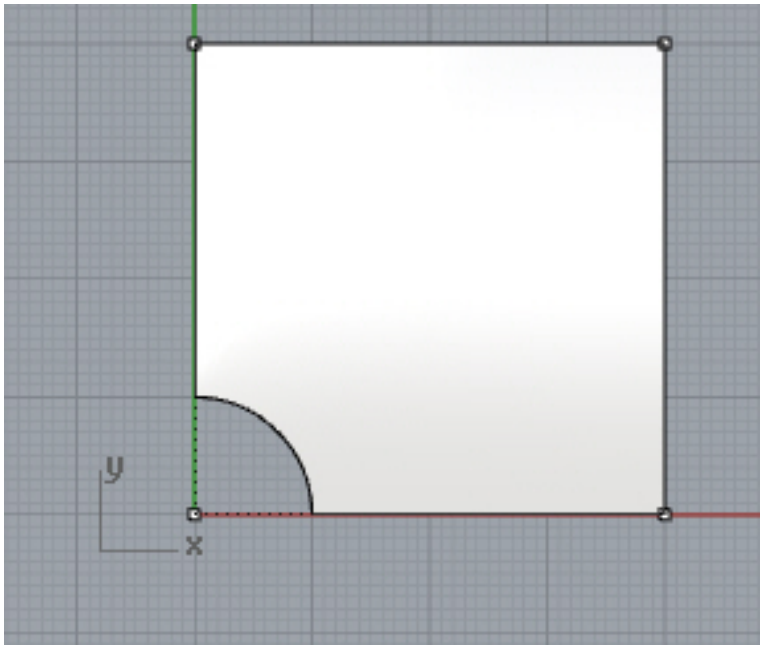

Figure 6.4: Trimmed surface from Rhino

The surface was also created without the use of trimming, shown in Figure 6.5

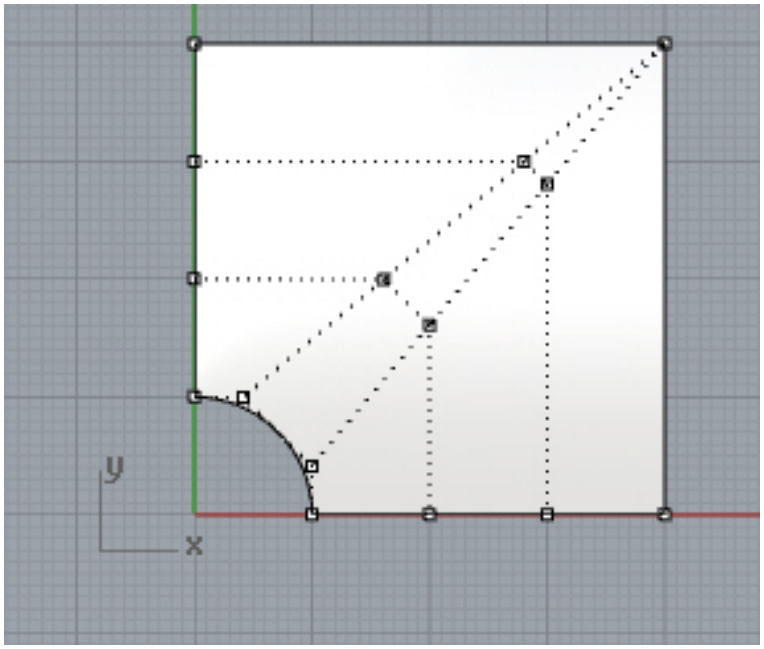

Figure 6.5: Untrimmed surface from Rhino

The untrimmed surface is analyzed using an existing matlab code which implements the theory behind NURBS surface shell analysis. The trimmed surface will be analyzed using my own matlab code for trimmed isogeometric elements elements, based on the theory discussed in this thesis. The trimmed surface is imported to the FE program Abaqus. Two of the meshes used in Abaqus are shown in Figure 6.6. The first mesh clearly shows how the surface is approximated using FEA.

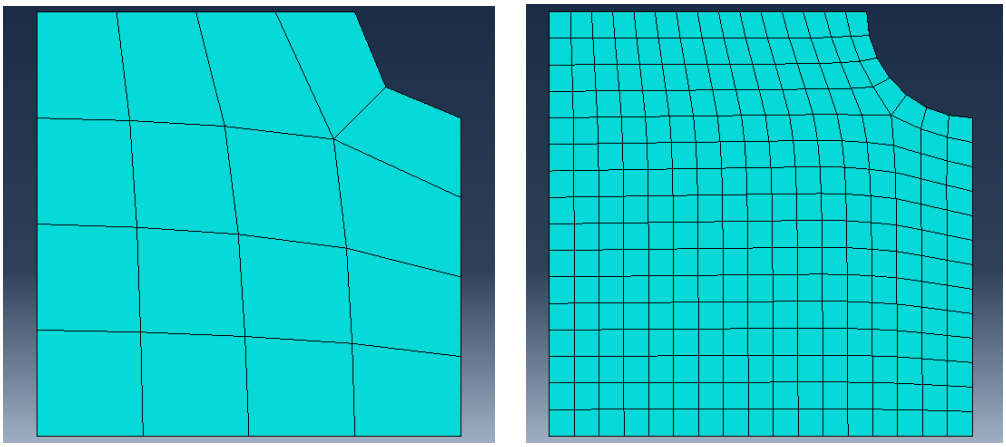

(a) (b)

Figure 6.6: Mesh of 4x4 and 16x16 elements in Abaqus

The displacements at the lower part of the edge imposed by a loading are compared for untrimmed IGA, trimmed IGA and FEA.

1Mesh size	11x1	12x2	14x4	18x8
Trimmed IGA	-0.0047	-0.0050	-0.0052	-0.0052
Untrimmed IGA	-0.0047	-0.0052	-0.0052	-0.0052
FEA	0.0033	-0.0039	-0.0050	-0.0052

The table above clearly show that IGA converges quicker than FEA. The untrimmed isogeometric surface reaches a converged soultion already at a mesh of only four elements. The finite element doesnt reach the same value untill the mesh is refined to 8x8 elements.

Stresses are also investigated for the plate. Since The untrimmed Nurbs surface is constructed with parametric coordinates s, and t it is difficult to compare the stresses to those for the model in Abaqus. This is because the s,t coordinates are not defined as the linear directions x,y,z. The trimmed NURBS surface however, has parametric coordinates s,t which behave linearly. This is because the surface is created as a rectangular surface and then trimmed. Because of this, it is possible to compare the stresses at a point on the trimmed IGA surface and the FE model. The stress component s_{uu} for the IGA model is compared to s_{11} from Abaqus. The results at the lower corner of the hole is presented in the table below.

1Mesh size	12x2	14x4	18x8	116x16	132x32
Trimmed IGA	61.4915	78.7546	82.4675	72.2577	71.6861
FEA	30.9218	35.7997	48.1502	59.9639	64.0063

A very fine mesh was also created in Abacus to verify the result, and act as a reference solution. At this mesh, the stresses had converges, which means the solution is accurate enough. The reference solution at this point was found to be s_{11}=71.6510 [Mpa]. The Nurbs surface does not differ too much from this solution for all meshes, and the final refinement of 32x32 elements lies within the boundary for an accurate solution. There is even a possibility that this solutions is more accurate than the one obtained from the FE surface. The stresses for the FEA has not yet reached an approximate solution, even for the finest mesh.

Chapter 7

Conclusion and further work

The mapping functions discussed work well for the cases looked at in this thesis. The quadrature points are shown to be mapped on to the active domain of trimmed elements. Implementation of the conditions for analysis can be complicated when taking into account all the possible integration domains.
So far, the Matlab code implementing the mapping and the element detection works for most element types that satisfy the conditions for analysis.
Further work could be done to account for more trimmed element cases, such as multiple trimming curves in one element, and elements with trimming curves which crosses an element edge in stead of a vertex. However, this would lead to a much more complex system and searching algorithms, so there might be advantageous to simply perform refinement of the surface for such cases. The method discussed which offers the lowest computational time is the NURBS enhanced triangles method. No knot insertion in necessary, unlike the other two.
This also saves computational effort, because there are fewer trimming curves and thereby fewer parameters to sort and keep track of during the integration.
However, there is more subdivision for this method, where elements of case 1 are divided into three parts, while elements of case 2 are divided into two. Some of these subdivisions may represent very small integration areas, which is unnecessary and might even be a disadvantage.
Further investigation into the subdivision of trimmed elements would be interesting. Some algorithm which determines the subdivision with the objective to find the most evenly distributed areas could be useful. In addition, the effect of trimmed elements which define notably small areas, could be investigated.
Are the integration of such elements harmful for the analysis, or just unnecessary use of computational time. Further, how small would the trimmed element have to be in relation to the rest, for it to be considered negligible. Analysis of a simple trimmed model using IGA, trimmed IGA and FEA proves that NURBS hold an advantage to Finite Elements because it represents an exact geometry. Trimmed analysis also proved to be a good method for analyzing the model. Futher investigation of trimmed analysis would be useful to identify a larger scope of its abilities. For example, if there are any elements which could not be analyzed using trimmed IGA. It would be interesting to look at more global components of ship hulls, and investigate how they all relate to form the global model.

List of Figures

Bibliography

[1] M. Breitenberger, A. Apostolatos, B. Philipp, R. Wuchner, K.-U. Bletzinger Analysis in computer aided design: Nonlinear isogeometric B-Rep analysis of shell structures *Comput. Methods Appl. Mech. Engrg.*, 284:401–457, (2015).

[2] M. Breitenberger CAD-integrated design and analysis of shell structures. Ph.D. thesis, Technical Universityof Munich, (2016)

[3] T. Hughes,J.A. Cottrell,Y. Bazilevs Isogeometric analysis: CAD, finite elements, NURBS, exact geometry and mesh refinement *Comput. Methods Appl. Mech. Engrg.*, 194:4135–4195, (2005).

[4] J. Kiendl. Isogeometric Analysis and Shape Optimal Design of Shell Structures, Technical University of Munich, (2010).

[5] G. Yujie , J. Heller, J.R. Hughes, M. Ruess, D. Schillinger Variationally consistent Isogeometric analysis of trimmed thin shells at finite deformations, based on the STEP exchange format, University of Aeronautics and Astronautics, Nanjing, P.R. China, (2017)

[6] H.J. Kim, Y. Seo, S. Youn Isogeometric analysis with trimming technique for problems of arbitrary complex topology *Comput. Methods Appl. Mech. Engrg.*, 199:2796–2812, (2010).

[7] H.J. Kim, Y. Seo, S. Youn Isogeometric analysis for trimmed CAD surfaces *Comput. Methods Appl. Mech. Engrg.*, 198:2882–2995, (2009).

[8] Y. Seo, H.J. Kim, S. Youn Isogeometric topology optimization using trimmed spline surfaces *Comput. Methods Appl. Mech. Engrg.*, 199:3270—3296, (2010).

[9] S.Timoshenko, S.Woinowsky-Krieger *LaTeX: Theory of plates and shells*, Mc.Graw-Hill, New York, 2nd edition, 1989.

[10] E. Ventsel, T.Krautehammer *LaTeX: Thin plates and shells: theory, analysis, and applications*, Marcel Dekker, New York, 2001.